NASA TECHNICAL MEMORANDUM 100629

ANALYSIS OF NOTCHED METAL MATRIX COMPOSITES UNDER TENSION LOADING

C. A. BIGELOW

JUNE 1988

National Aeronautics and
Space Administration

Langley Research Center
Hampton, Virginia 23665-5225

SUMMARY

This paper presented analytical results from a three-dimensional finite element analysis, which uses a vanishing-fiber-diameter material model. One very attractive feature of this program is that it requires only the properties of the individual constituents to conduct an analysis of any metal matrix laminate. Additionally, PAFAC calculates the fiber stresses in each element. Examples are shown for specific metal matrix composites such as boron/aluminum and silicon-carbide/aluminum. However, the analysis and techniques described can be applied to any combination of matrix and continuous fiber.

Specimen stress-strain behavior and stress at first fiber failure were predicted for boron/aluminum laminates containing circular holes and crack-like slits. The predictions compared very well with test data for laminates containing 0^0 fibers and reasonably well for $[\pm 45]_{2s}$ laminates. Mesh configuration was shown to have an effect on the calculation of stresses local to the notch. The presence of thin interface layers of matrix material had a significant influence on the slit tip stress state, causing sharper stress gradients near the notch. Interface layers reduced the slit-tip fibers stresses in a $[\pm 45]_s$ silicon-carbide/aluminum laminate but increased them in a $[0/90]_s$ laminate.

The results presented here show that the analysis of metal matrix composites is not trivial. Many aspects of the analysis (e.g., mesh geometry, interface layers, material properties) can have a significant influence on the stress state local to the notch.

INTRODUCTION

Metal matrix composites have several inherent properties, such as high stiffness-to-weight ratios and high strength-to-weight ratios, which make them attractive for structural applications. These composites also have greater transverse strength, a higher operating temperature range, and better environmental resistance than current polymer matrix composites. Like polymer matrix composites, however, metal matrix composites are very notch sensitive. The degree of this sensitivity depends on notch size and shape, as well as the laminate orientation. Unlike typical polymer matrix composites, metal matrix composites may exhibit wide spread yielding of the matrix before laminate failure. To design damage-tolerant structures (or to simply understand the effects of fastener holes), the laminate fracture strengths must be known for a wide range of ply orientations, notch geometries, and loading conditions. A method for predicting fracture strength is needed to avoid testing all the laminate, notch, and loading combinations of interest.

In metal matrix composites the matrix may yield, whereas the fibers remain elastic until they fracture. An analysis that models this two phase behavior for any specimen configuration and incorporates fiber failure was presented in [1]. The analysis is a three-dimensional finite element program [2] called PAFAC (Plastic and Failure Analysis of Composites). The PAFAC program uses the vanishing-fiber-diameter continuum model developed by Bahei-El-Din and Dvorak [3-5] to represent the essential aspects of the elastic-plastic behavior of the composite lamina.

This paper will first present a brief description of the PAFAC finite element program and review some past work using the program. Then the results of some current work will be presented. The effects of mesh configuration on slit tip stress concentrations and fiber failure will be discussed. The effect

of modeling thin layers of matrix material between each orthotropic lamina will be discussed.

ANALYTICAL MODELING OF FIBROUS COMPOSITES

In metal matrix composites, the matrix yields, whereas the fibers generally behave elastically until they break. To model the behavior of metal matrix composites, the elastic-plastic behavior of the matrix and the elastic behavior of the fiber should be accounted for. An analysis that models this two phase behavior was used in the present study. This analysis was conducted with a three-dimensional finite element program [2] called PAFAC, which was developed from a program written by Bahei-El-Din et al. [3,6]. PAFAC uses a constant strain, eight-noded, hexahedral element. Each hexahedral element represents a unidirectional composite material whose fibers can be oriented in the appropriate direction in the structural (Cartesian) coordinate system.

Material Model

The PAFAC program uses a vanishing-fiber-diameter material model developed by Bahei-El-Din and Dvorak [3-5] to represent the essential aspects of the elastic-plastic behavior of the composite lamina. The material model is briefly described in the appendix. This material model requires only the material properties of the fiber and matrix to predict the laminate response. The program is able to calculate the fiber stresses in each element from the material model. Further details on the material model can be found in [3-5].

Finite Element Model

All the specimens analyzed contained center notches, either circular holes or crack-like slits. A typical specimen with a crack-like center slit is shown

in Figure 1. Two typical finite element meshes, a radial mesh and a rectangular mesh, are shown in Figures 2 and 3. Typically, a mesh consisted of 2250 nodes and 1392 elements, although this varied depending on the number of plies and specimen configuration. In all cases, only one-eighth of the specimen was modeled because of symmetry. A uniform stress was applied to the end of the specimen to simulate tensile loading.

At least one layer of elements is needed for every ply angle in the laminate. For example, a $[0]_6$ laminate could be modeled by one layer of elements, while a $[0/\pm45]_s$ would require at least three layers of elements. Unless otherwise stated, each ply of the laminates was modeled with one layer of elements.

Fiber Failure Criteria

The following equation, developed by Johnson et al. [1], is used as the fiber failure criterion in the PAFAC program:

$$\left[\frac{\sigma_{33}^{f}}{\sigma_{33}^{ult}}\right]^2 + \left[\frac{\sigma_{13}^{f}}{\sigma_{13}^{ult}}\right]^2 \geq 1 \qquad (1)$$

In this equation, the subscript 3 represents the fiber axial direction and 1 represents the transverse direction. σ_{33}^{f} represents the current tensile stress in the fiber and σ_{13}^{f} represents the current shear stress in the fiber. The ultimate strengths of the fiber in the tensile and shear modes are σ_{33}^{ult} and σ_{13}^{ult}, respectively. Previous analysis [1] did not use a mesh fine enough to model an element with a width of one fiber spacing. Thus, instead of using the ultimate tensile strength of a single fiber, an averaging technique was used in

[1] to determine the fiber ultimate strengths in the tensile and shear modes. Since two strengths are unknown, two test cases were required. The monolayer with a slit and a $[\pm 45]_{2s}$ specimen containing a hole were used. These two layups were chosen because the dominant fiber stress at the slit tip in the monolayer is the tensile stress σ_{33}^{f}, while in the $[\pm 45]_{2s}$ laminate the dominant fiber stress is the shear stress σ_{13}^{f}. From radiographs [1], the laminate stress at first fiber failure could be closely estimated. The finite element model for each laminate configuration was loaded to the stress level where first fiber failure occurred. The corresponding fiber stresses σ_{33}^{f} and σ_{13}^{f} were recorded for the element where first fiber failure was observed. The pairs of σ_{33}^{f} and σ_{13}^{f} were substituted into equation (1) and the equation was solved for the two unknowns, σ_{33}^{ult} and σ_{13}^{ult}. This gave values of 2500 MPa and 100 MPa for σ_{33}^{ult} and σ_{33}^{ult}, respectively. First fiber failure was predicted for boron/aluminum specimens containing either circular holes or crack-like slits in [1] using these values.

NOTCH STRENGTH

The PAFAC program was used to predict the stress-strain behavior and first fiber failure of boron/aluminum laminates with either circular holes or crack-like slits [1]. Material properties of the boron and aluminum are given in Table 1. This section will summarize the results presented in [1].

Specimens With Holes

The overall stress-strain behavior and first fiber failure were predicted for $[0]_6$, $[0/\pm 45]_s$, $[0_2/\pm 45]_s$, $[\pm 45]_{2s}$ boron/aluminum laminates containing circular holes in [1]. In Figure 4 the applied stress is plotted against the specimen overall strain for a $[0/\pm 45]_s$ laminate containing a circular hole. The

solid line represents the predicted response up to first fiber failure. The symbols represent experimental data. There is excellent correlation between the predicted and the experimental stress-strain behavior. First fiber failure was predicted to occur near laminate failure. First fiber failure was not observed for this laminate [1] and therefore was assumed to occur at laminate failure. The first fiber failure was predicted next to the hole in the 0^0 ply element on the transverse axis, as shown in the sketch. Figure 5 summarizes the first fiber failure predictions for the specimens containing circular holes. Predictions for the other layups agreed well with the experimental data.

Specimens With Slits

The PAFAC analysis was also used to predict first fiber failure and overall stress-strain behavior for several boron/aluminum laminates containing crack-like slits [1]. Figure 6 compares the analytical and experimental results for a $[0/\pm45]_s$ specimen containing a center slit. The predicted stress-strain response agreed very well with the experimental data. The predicted first fiber failure was very close to the laminate failure stress. Figure 7 summarizes the first fiber failure predictions for the specimens containing crack-like slits. Except for the $[0]_6$, predictions for the other layups agreed well with the experimental data.

EFFECT OF MESH CONFIGURATION

It is well known that unidirectional laminates develop long, narrow plastic zones at the slit tip due to the intense shear stresses. These zones, parallel to the fibers, were noted by Goree and Jones [7] and are shown in Figure 8. However, it is not so well known that these zones of intense shear stresses would be present in slit laminates containing both 0^0 and angle plies. As shown

in Figure 9, Post et al. [8] found rather significant shear zones at a slit tip in a $[0/\pm45]_s$ boron/aluminum laminate. Previous PAFAC analyses [1,2] used a radial mesh, such as shown in Figure 2. Because of the configuration of the mesh above the slit tip, the radial mesh could not predict the intense shear stresses parallel to the fibers in the 0^0 direction. A rectangular mesh, with a rectangular slit tip, was then used [9] to capture these zones of high shear.

In [9], five layups of silicon-carbide/aluminum ($[0]_8$, $[0_2/\pm45]_s$, $[0/90]_{2s}$, $[0/\pm45/90]_s$, and $[\pm45]_{2s}$) with slits were tested statically to failure. The strain distribution ahead of the slit tip was found experimentally with a series of strain gages bonded ahead of the slit tip. For all layups, except the $[0]_8$, the yielding of the metal matrix caused the fiber stress concentration factor to increase with increasing load. This is contrary to behavior seen in homogeneous materials where yielding causes the stress concentration to drop. For the $[0]_8$ laminate, yielding of the matrix was found to cause a decrease in the fiber stress concentration. The strain distribution ahead of the slit was also predicted with the PAFAC analysis using a rectangular mesh such as shown in Figure 3. For all layups, the finite element analysis, using the rectangular mesh, predicted the experimental trends correctly. The predictions made with the radial mesh, however, were in error, predicting that the fiber stress concentration in the $[0]_8$ laminate would increase due to yielding.

The effect of the mesh in the slit tip region is further investigated here. The two meshes shown in Figures 2 and 3, as well as the mesh in Figure 10, were used. The mesh shown in Figure 10 was formed to combine a curved slit tip with a rectangular mesh. In these figures, due to symmetry, only one quarter of the plan view of the mesh is shown. Each figure also shows the slit-tip detail for each mesh. In all three meshes, the slit-tip element has the same width

(dimension in the x-direction). The slit-tip element was sized to represent one fiber spacing (0.192 mm).

Notch Tip Stresses

The three meshes were used to analyze a unidirectional boron/aluminum monolayer with a center slit. The material properties are given in Table 1. The specimen was 76 mm wide with a slit length of 19 mm. The different mesh configurations did not have any effect on the overall stress-strain behavior of specimen. The major difference was seen near the slit tip. Figure 11 compares the distributions of the stress in the loading direction ahead of the slit tip for the meshes shown in Figures 2, 3, and 10. At the slit tip, the stresses computed with the two rectangular meshes, for both the laminate and the fiber, are significantly higher than computed with the radial mesh. Stresses are calculated at the element centroid. Although all the slit-tip elements are the same size in the x-direction (parallel to the slit), the slit tip element in the radial mesh does not have the same dimensions in the y-direction (perpendicular to the slit) as in the rectangular meshes. This difference is shown in Figures 2, 3, and 10 in the sketch of the slit tip elements. Thus the location of the stress for the radial mesh is slightly different than for the two rectangular meshes. Because of the very steep stress gradients at the slit tip, even a small difference in location may have a significant effect on the stress calculations. Away from the slit tip, all three meshes agree even though again the locations of the stresses are different for the radial mesh. The results computed using the rectangular mesh with the rectangular slit tip and with the curved slit tip are nearly identical. Thus, for the remainder of this paper, the only rectangular mesh used will be the one with the rectangular slit tip.

Figures 12 and 13 show the σ_y stress contours for the radial and rectangular meshes shown in Figures 2 and 3, respectively. Due to symmetry conditions, only one quarter of the plan view of the specimen is shown in the stress contours. Figures 14 and 15 show the τ_{xy} stress contours for the meshes shown in Figures 2 and 3, respectively. By comparing Figure 12 to 13 and 14 to 15, it is obvious that the radial mesh cannot model the shear band. The stress contours were significantly affected by the mesh configuration. The radial mesh (Figure 2) could not model the high shear zones present in the unidirectional specimen.

Fiber Failure Strengths

Since the rectangular mesh has a slit-tip element sized to contain one fiber, new values of σ_{33}^{ult} and σ_{13}^{ult} should be calculated. The averaging technique, as described above and in [1], was used. It was anticipated that now σ_{33}^{ult} would represent the ultimate tensile strength of a single fiber. Values of 5300 MPa and 40 MPa were found for σ_{33}^{ult} and σ_{13}^{ult}, respectively. This value of σ_{33}^{ult} is rather large compared to the tensile ultimate strength of the boron fiber of 3160 MPa [10]. However, this value of ultimate strength for the boron fiber was obtained from tensile tests of unnotched 0^0 boron/aluminum specimens [10] in which a relatively large volume of material was subjected to a uniform stress. For the specimens with a notch the material next to the notch is subjected to a stress gradient and the peak stress exists only over a small volume. Thus, σ_{33}^{ult} may exceed the fiber ultimate tensile strength.

Using the fiber ultimate strengths of 5300 and 400 MPa in Eqn. (1) with the rectangular slit-tip mesh (Figure 3), first fiber failure was predicted for two laminates with slit-like slits previously analysed in [1] using a radial mesh. However, the new predictions of first fiber failure were grossly in error,

predicting first fiber failure at stress levels that were much too low. These erroneous predictions may have been due to mesh effects. The rectangular mesh models the shear stresses well but may not model other aspects as adequately. More work will be done in this area.

EFFECT OF MATRIX INTERFACE LAYERS

In [11] Guo, Post, and Czarnek compared Moire fringe patterns for a $[0/\pm45]_s$ and a $[\pm45/0_2]_s$ laminate, both center notched tensile specimens made of boron/aluminum. Figure 16 compares the fringe patterns of y-displacements for the two specimens. The two fringe patterns have similar global deformations (Figure 16(a) and 16(c)). As stated in [11], this indicates that the successive plies of different orientations constrain each other by the interlaminar shear stresses acting in the matrix layers between the plies causing them to deform together. However, the local displacements at the slit tip (Figures 16(b) and 16(d)) are very different. There was no evidence of delamination; therefore, strong shear strains must exist in the matrix layers between plies to maintain continuity.

To account for this effect in the analysis, a thin isotropic layer of matrix material was modeled between each layer of orthotropic material. Two silicon-carbide/aluminum laminates were analyzed: $[\pm45]_s$ and $[0/90]_s$. The material properties are given in Table 1. For each laminate, three cases were compared, no isotropic layers, one isotropic layer, and three isotropic layers modeling the interface layer. The model is shown schematically in Figure 17 for a [0/90] laminate. (The laminate in Figure 17 has only two plies for simplicity.) The thickness of the interface layer was chosen to be 0.03175 mm (typical fiber spacing for silicon-carbide/aluminum) and the fiber volume fraction of the orthotropic layers was adjusted to maintain a laminate fiber

volume fraction of 0.44. The interface shown in Figure 17 was modeled with one or three layers of elements. The specimen was 51-mm wide, 164-mm long with a slit 19-mm long in the center.

As expected, the overall stress-strain behavior of the specimens for either layup were not changed by including interface layers in the model. However, the stress gradients in the area of the slit tip and fiber stresses in the slit tip element were significantly affected.

$[\pm 45]_s$ Laminate

Figure 18 compares the stress contours for σ_y for the three models for the $+45^0$ layer in the $[\pm 45]_s$ laminate at an applied stress of 60 MPa. At this level of applied stress there is global yielding in the specimen. Figure 18(a) presents the σ_y stress contours for the $[\pm 45]_s$ laminate with no interface layers, 18(b) presents the contours for the laminate with one interface layers, and 18(c) presents contours for the laminate with three interface layers. As shown in the figure, adding the interface layers allowed the two layers of the laminate to displace relative to one another, resulting in sharper stress gradients above the slit tip. Figure 18 shows that not only is there a much sharper gradient above the slit tip but the stress contours above the slit are also more compressed by adding the interface layers. Similar behavior was seen for the shear stress components, as shown in Figure 19 for the τ_{xy} stress in the 45^0 layer in the $[\pm 45]_s$ laminate.

Including interface layers also had an effect on the fiber stress in the element at the slit tip. Figure 20 shows the axial component of slit-tip fiber stresses for the -45^0 layer of the $[\pm 45]_s$ laminate at an applied stress of 60 MPa. Here the presence of the interface layers caused the fiber stresses to drop significantly, about 30% for the three interface layer case. Including

three interface layers reduced the shear component of the fiber stress at the slit tip by about 3%.

$[0/90]_s$ Laminate

Figure 21 presents the σ_y stress contours in the 0^0 layer of a $[0/90]_s$ laminate for an applied stress of 110 MPa. A similar trend is seen here. By adding interface layers, the stress contours are more compressed. Also notice that in the area above the slit that the stresses were lowered by adding the interface layers. The presence of the interface layers allows the two plies to act more independently; thus, the 0^0 layer of the $[0/90]_s$ laminate now acts more like a monolayer. Figure 22 shows the fiber axial stresses in the slit-tip in the 0^0 layer for the $[0/90]_s$ laminate at an applied stress of 110 MPa. For the $[0/90]_s$ laminate, the interface layers caused an increase of about 15% in the fiber stresses at the slit-tip. The interface layers allowed the 0^0 layers to experience less constraint from the 90^0 layers, thus producing a higher fiber stresses.

CONCLUDING REMARKS

This paper presented analytical results from a three-dimensional finite element analysis, which uses a vanishing-fiber-diameter material model. One very attractive feature of this program is that it requires only the properties of the individual constituents to conduct an analysis of any metal matrix laminate. Additionally, PAFAC calculates the fiber stresses in each element. Examples are shown for specific metal matrix composites such as boron/aluminum and silicon-carbide/aluminum. However, the analysis and techniques described can be applied to any combination of matrix and continuous fiber.

Specimen stress-strain behavior and stress at first fiber failure were predicted for boron/aluminum laminates containing circular holes and crack-like slits. The predicted stress-strain response and stress at first fiber failure compared very well with test data from laminates containing 0^0 fibers and reasonably well for $[\pm 45]_{2s}$ laminates.

It was shown that the mesh configuration can have an effect on the calculation of the stress distribution in the notch region. The kinematics of the problem must be considered when determining the mesh configuration.

The presence of thin interface layers of matrix material had a significant influence on the calculated slit tip stress state in silicon-carbide/aluminum laminates, causing sharper stress gradients and allowing each ply to act more independently. Interface layers reduced the slit-tip fibers stresses by 30% in a $[\pm 45]_s$ silicon-carbide/aluminum laminate but increased the slit-tip fiber stress by 15% in a $[0/90]_s$ silicon-carbide/aluminum laminate.

The results presented here show that the analysis of metal matrix composites is by no means trivial. Many aspects of the analysis (e.g., mesh geometry, interface layers, material properties) can have a significant influence on the stress state local to the notch.

REFERENCES

1. Johnson, W. S.; Bigelow, C. A.; and Bahei-El-Din, Y. A.: Experimental and Analytical Investigation of the Fracture Processes of Boron/ Aluminum Laminates Containing Notches. NASA TP-2187, National Aeronautics and Space Administration, Washington, D.C., 1983.

2. Bigelow, C. A.; and Bahei-El-Din, Y. A.: Plastic and Failure Analysis of Composites (PAFAC). LAR-13183, COSMIC, University of Georgia, 1983.

3. Bahei-El-Din, Y. A.: Plastic Analysis of Metal-Matrix Composite Laminates. Ph.D. Dissertation, Duke University, 1979.

4. Dvorak, G. J.; and Bahei-El-Din, Y. A.: Plasticity of Composite Laminates. Research Workshop on Mechanics of Composite Materials, Duke University, October 1978, pp. 32-54.

5. Bahei-El-Din, Y. A.; and Dvorak, G. J.: Plastic Yielding at a Circular Hole in a Laminated FP-Al Plate. Modern Developments in Composite Materials and Structures, J. R. Vinson, Ed., American Society of Mechanical Engineers, c. 1979, pp. 123-147.

6. Bahei-El-Din, Y. A.; Dvorak, G. J.; and Utku, S.: Finite Element Analysis of Elastic-Plastic Fibrous Composite Structures. Computers and Structures, vol. 13, no. 1-3, June 1981, pp. 321-330.

7. Goree, J. G.; and Jones, W. F.: Fracture Behavior of Unidirectional Boron/ Aluminum Composite Laminates. NASA CR-3753, National Aeronautics and Space Administration, Washington, DC, December 1983.

8. Post, D.; Czarnek, R.; Joh, D.; Jo, J.; and Guo, Y.: Elastic-Plastic Deformation of a Metal-Matrix Composite Coupon With a Center Slot. NASA CR-178013, National Aeronautics and Space Administration, Washington, D.C., November, 1985.

9. Johnson, W. S.; and Bigelow, C. A.: Elastic-Plastic Stress Concentrations Around Crack-Like Notches in Continuous Fiber Reinforced Metal Matrix Composites. NASA TM-89093, National Aeronautics and Space Administration, Washington, D.C., February 1987.

10. Sova, J. A.; and Poe, C. C.: Tensile Stress-Strain Behavior of Boron/Aluminum Laminates. NASA TP-1117, 1978.

11. Guo, Y.; Post, D.; and Czarnek, R.: Deformation Analysis of Metal Matrix Specimens By Moire Interferometry, Proceedings of the Fourth Annual Review, Virginia Tech Center for Composite Materials and Structures, May 11-17, 1987, Virginia Polytechnic Institute and State University, Blacksburg, VA 24601

APPENDIX - MATERIAL MODEL OF PAFAC PROGRAM

The PAFAC program uses a vanishing-fiber-diameter material model developed by Bahei-El-Din and Dvorak [3-5] to represent the essential aspects of the elastic-plastic behavior of the composite lamina. The material model is briefly described in this appendix.

The model consists of an elastic-plastic matrix unidirectionally reinforced by continuous elastic fibers. Both constituents are assumed to be homogeneous and isotropic. The fibers are assumed to have a very small diameter, so that although the fibers occupy a finite volume fraction of the composite, they do not interfere with matrix deformation in the two transverse directions, but only in the axial (fiber) direction. This assumption is generally referred to as the vanishing-fiber-diameter model. Figure 22 shows a schematic of this lamina model. In Figure 22, the x_1, x_2, and x_3 axes are the element coordinate system. In Figure 22, the fiber (axial) direction is parallel to the x_3-axis, and the x_1- and x_2-axes represent the transverse directions. The lamina model can also be represented by parallel fiber and matrix bars or plates with axial coupling, as illustrated in Figure 22.

If the Cartesian coordinates are chosen so the x_3 coincides with the fiber direction, the second-order tensors of the independent stress and strain components, σ and ϵ, are expressed as

$$\sigma = [\sigma_{11} \quad \sigma_{22} \quad \sigma_{33} \quad \sigma_{12} \quad \sigma_{13} \quad \sigma_{23}]^T$$
$$\epsilon = [\epsilon_{11} \quad \epsilon_{22} \quad \epsilon_{33} \quad \gamma_{12} \quad \gamma_{13} \quad \gamma_{23}]^T$$

where $\gamma_{ij} = 2\epsilon_{ij}$ $(i, j = 1, 2, 3;\ i \neq j)$ are the engineering shear strain components.

For equilibrium and compatibility, several requirements are imposed on the material model shown in Figure 22. The only constraint in the model is in the axial (fiber) direction; the matrix and fiber must deform equally. Thus,

$$\bar{\epsilon}_{33} = (\epsilon_{33})_f = (\epsilon_{33})_m$$

The stress average in each constituent can be related to the overall composite stress $\bar{\sigma}$ in the axial (fiber) direction as follows:

$$\bar{\sigma}_{33} = v_f(\sigma_{33})_f + v_m(\sigma_{33})_m$$

A bar over a symbol indicates overall composite stress or strain, and the subscripts f and m denote quantities related to the fiber and matrix. The volume fractions v_f and v_m are such that $v_f + v_m = 1$. In this material model, the other stress components in each constituent are assumed to be uniform and to obey the following equilibrium equations:

$$\bar{\sigma}_{11} = (\sigma_{11})_f = (\sigma_{11})_m$$
$$\bar{\sigma}_{22} = (\sigma_{22})_f = (\sigma_{22})_m$$
$$\bar{\sigma}_{12} = (\sigma_{12})_f = (\sigma_{12})_m$$
$$\bar{\sigma}_{13} = (\sigma_{13})_f = (\sigma_{13})_m$$
$$\bar{\sigma}_{23} = (\sigma_{23})_f = (\sigma_{23})_m$$

The other strain components can be related to the overall strain, $\bar{\epsilon}$ as follows:

$$\bar{\epsilon}_{ij} = v_f(\epsilon_{ij})_f + v_m(\epsilon_{ij})_m \qquad (ij \neq 33)$$

Since the fibers are elastic up to failure, the inelastic strains of the lamina are caused by matrix deformation. Because the fiber imposes an elastic constraint on the matrix which affects the shape of the lamina yield surface, additional kinematic components appear in the hardening rule of the lamina and influence the magnitude of the overall plastic strains. All aspects of the yield behavior were examined and accounted for in the formulation of the lamina constitutive equations. These equations are explicitly described in [2,3]. The stress-strain curve of the matrix material was modeled with a Ramberg-Osgood equation. The slope of the effective stress-effective plastic strain curve H was calculated using the following equation:

$$H = (3\ G/n/\kappa)\ (\sigma_{ys}/\sigma^{m}_{eff})^{(n-1)}$$

where σ^{m}_{eff} is the effective stress in the matrix material, σ_{ys} is the yield stress of the matrix material, G is the shear modulus of the matrix material, and n and κ are determined by fitting experimental data. For the 6061 aluminum matrix material, G = 27200 MPa, σ_{ys} = 34.5 MPa, n = 5.5, and κ = 0.05.

Table 1 - Constituent Properties

Material	Modulus, GPa	Poisson's Ratio	Yield Strength, MPa
Aluminum, 6061	72.3	0.33	34.5
Boron	400	0.13	--
Silicon-Carbide	340	0.25	--

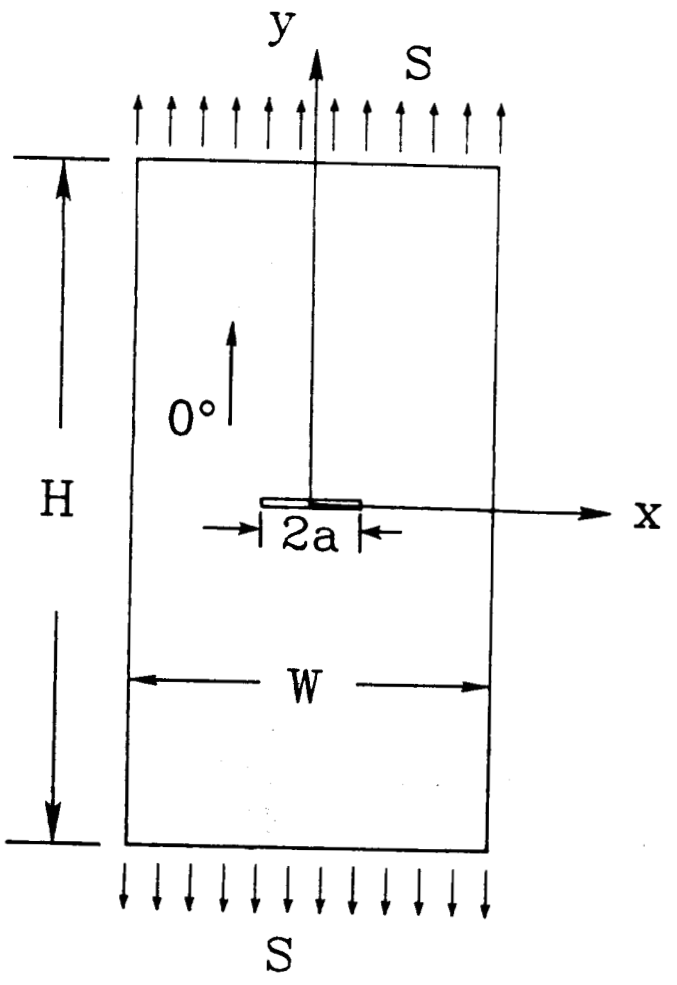

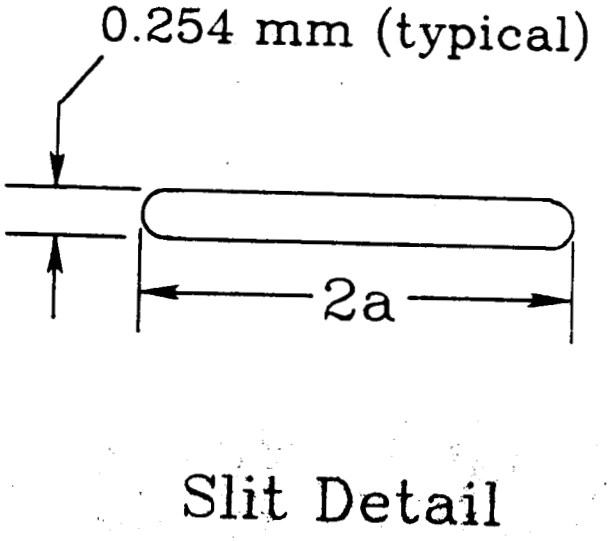

Figure 1. Typical specimen configuration with a crack-like slit.

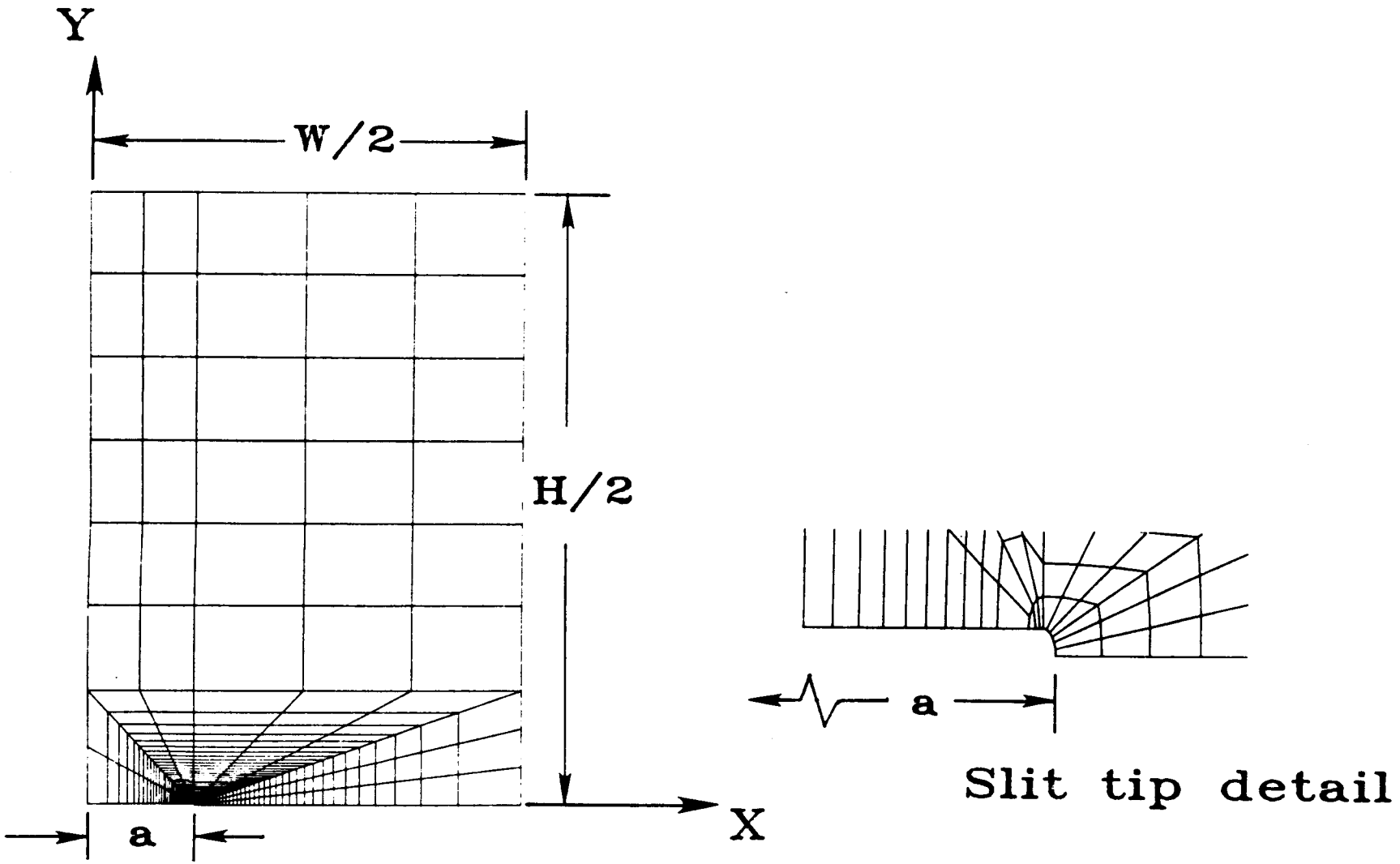

Figure 2. Radial finite element mesh. 2a = 19 mm, W = 78 mm, and H = 101 mm.

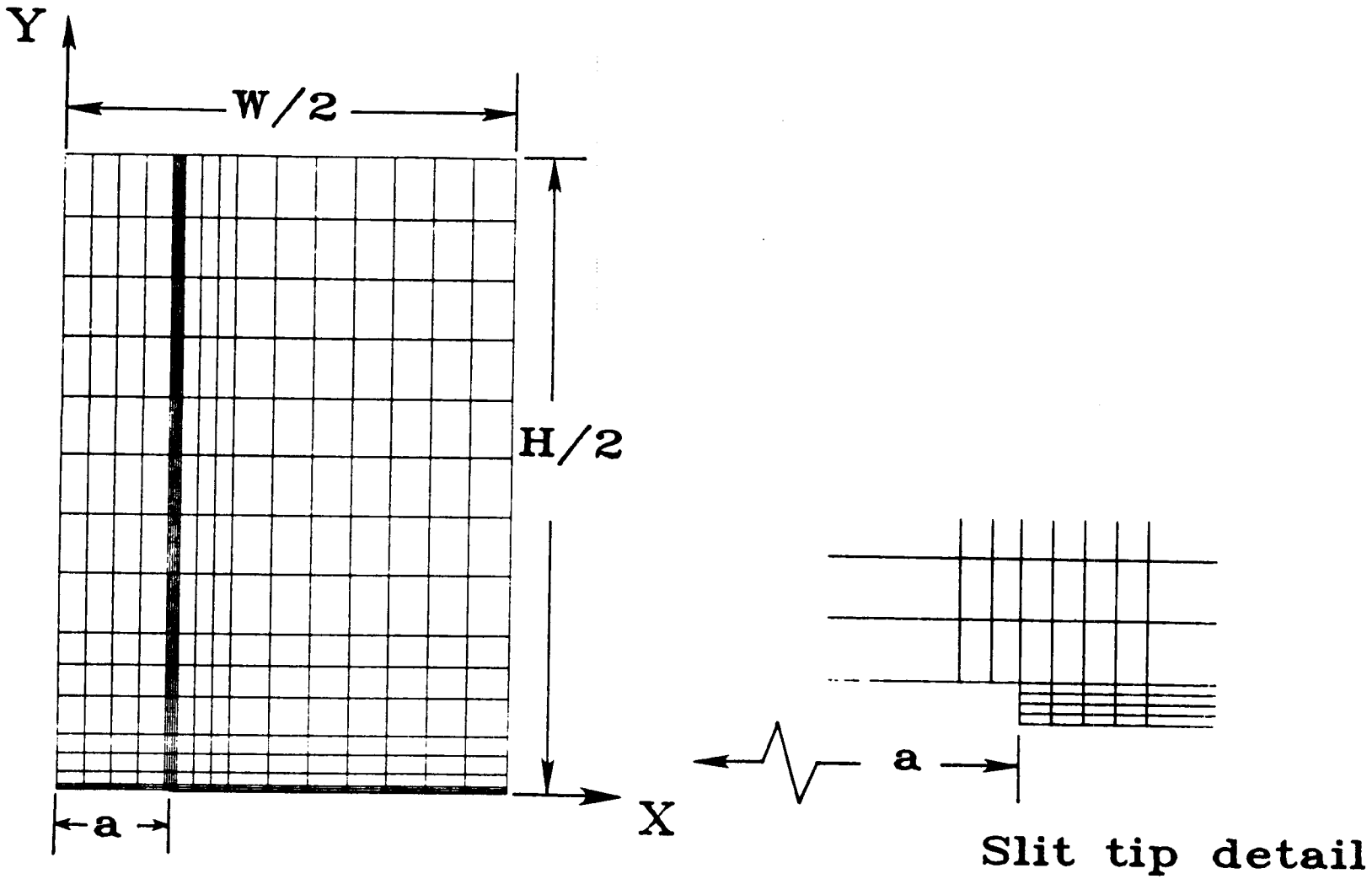

Figure 3. Rectangular mesh with rectangular slit tip. 2a = 19 mm, W = 78 mm, and H = 101 mm.

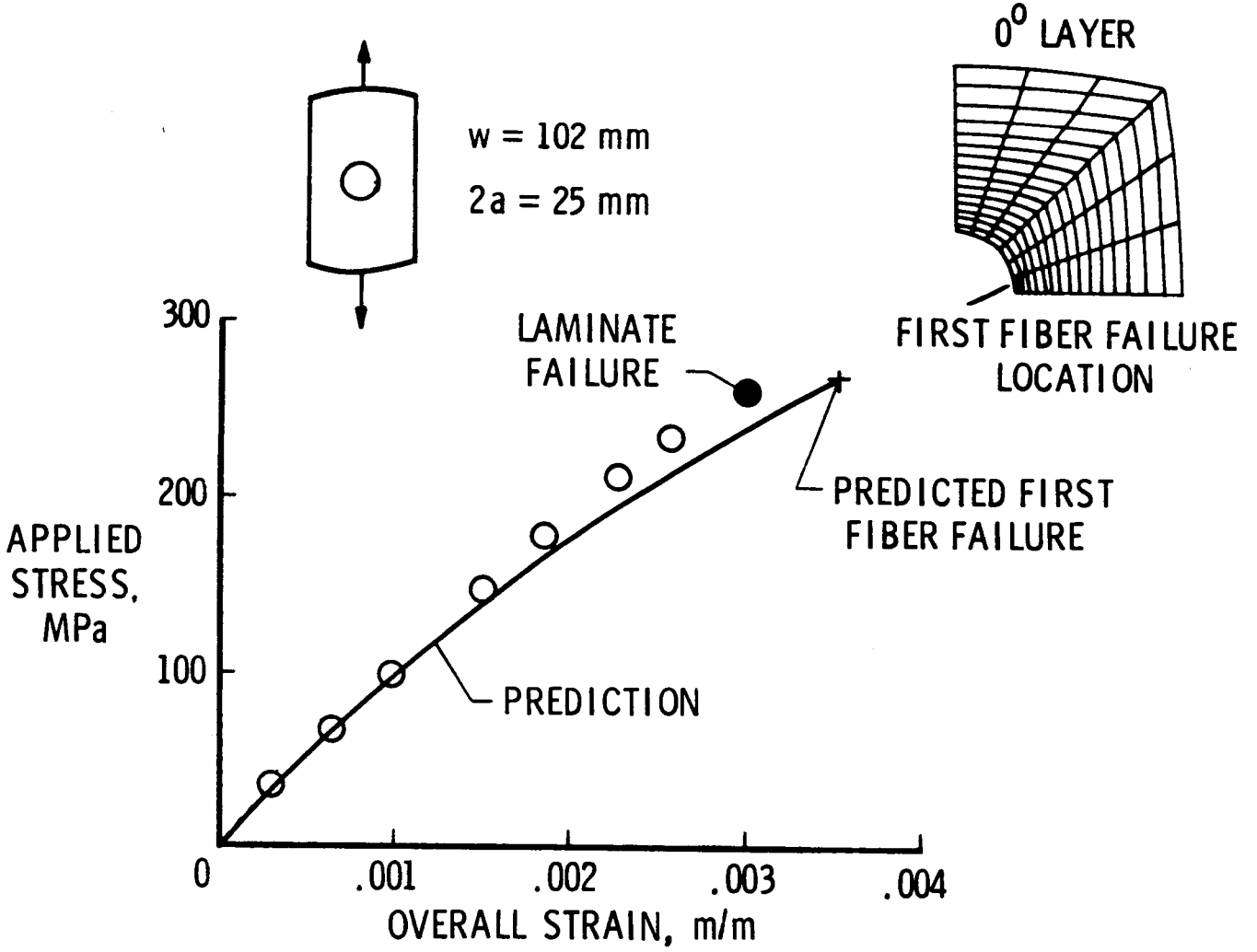

Figure 4. Stress-strain response to failure of $[0/\pm45]_s$ laminate with circular hole. 2a = 25.4 mm; w = 102 mm.

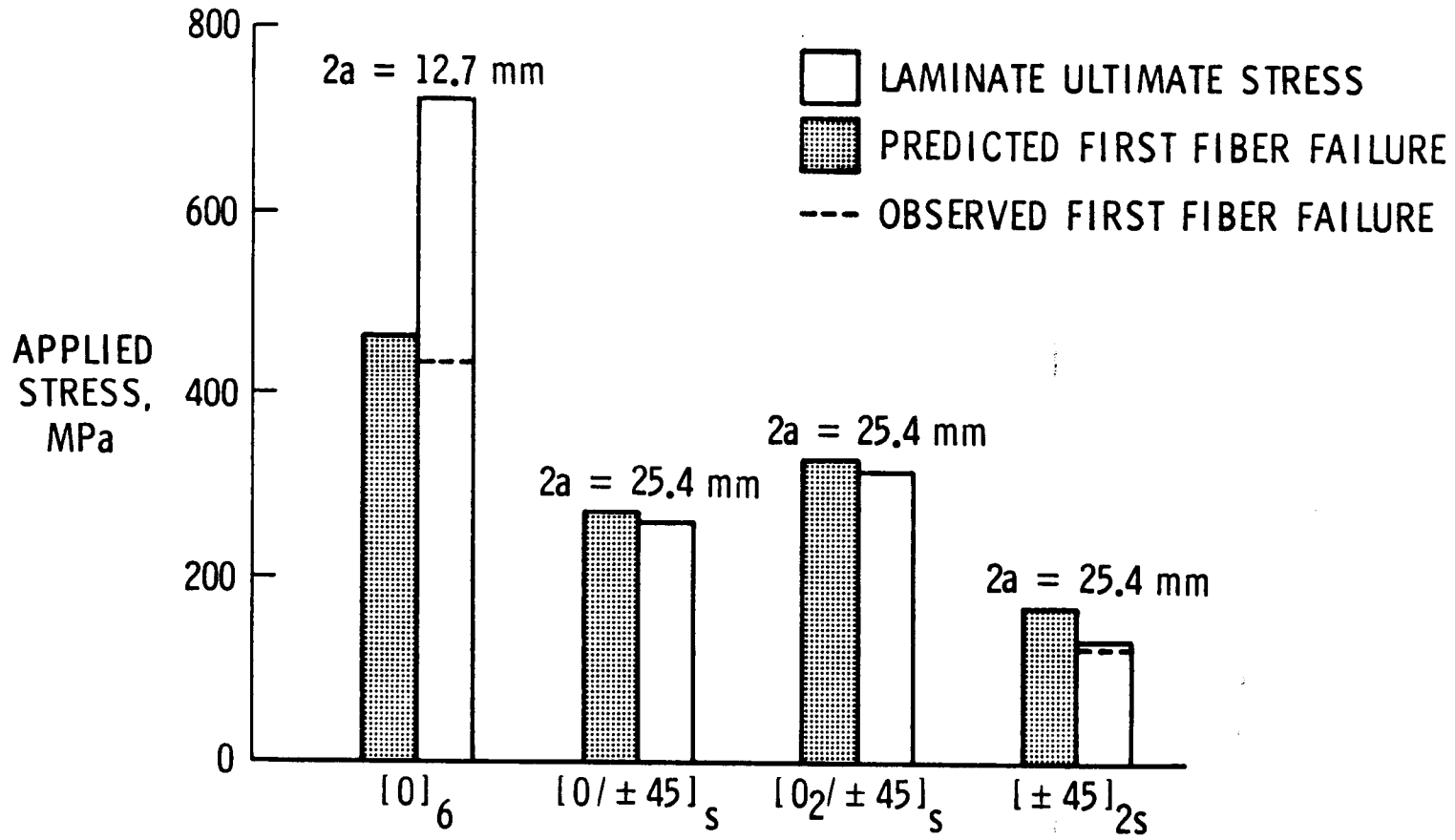

Figure 5. First fiber failure compared with laminate ultimate stress for specimens with circular holes. W = 102 mm.

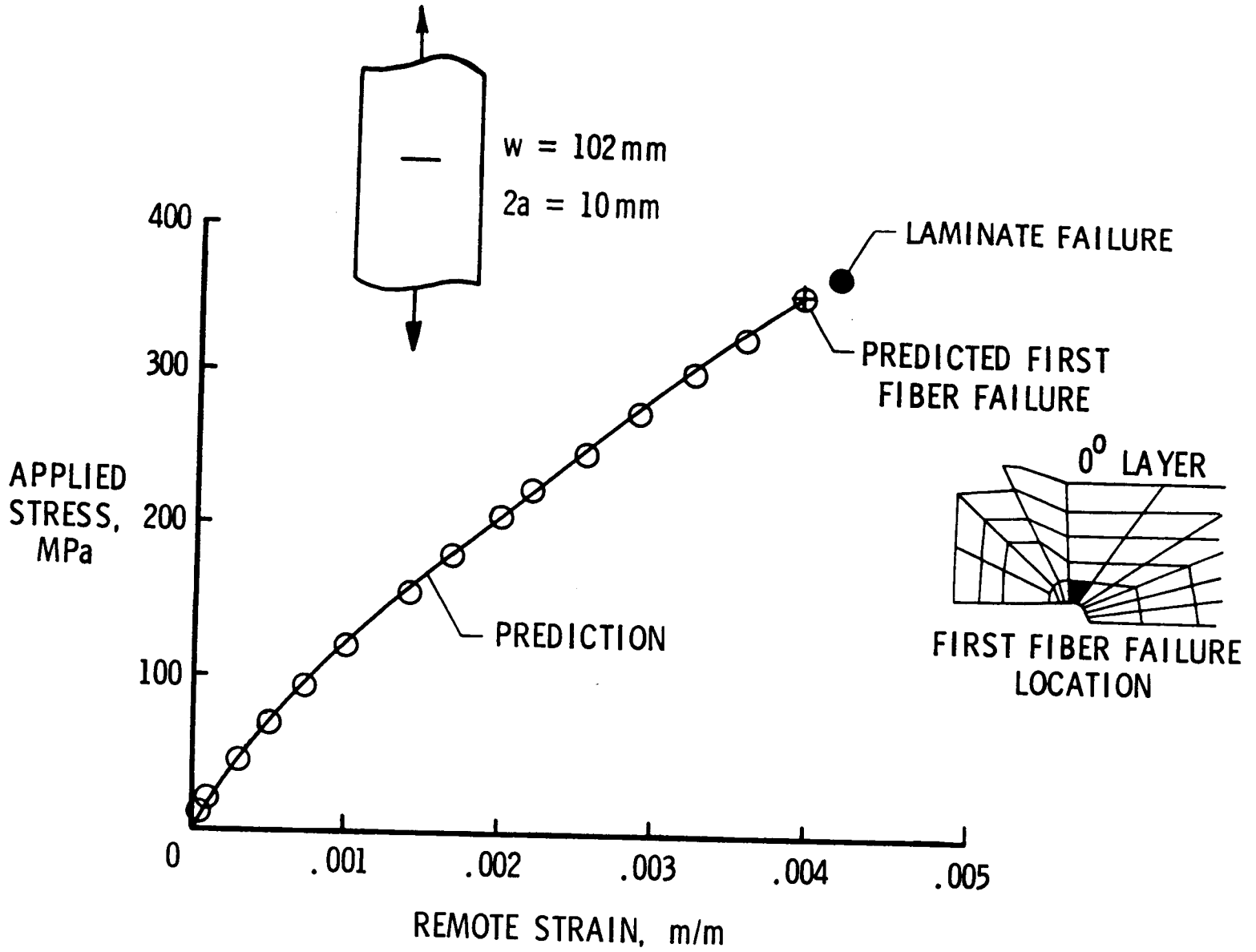

Figure 6. Stress-strain response to failure of $[0/\pm45]_s$ laminate with crack-like slit. 2a = 10 mm; w = 102 mm.

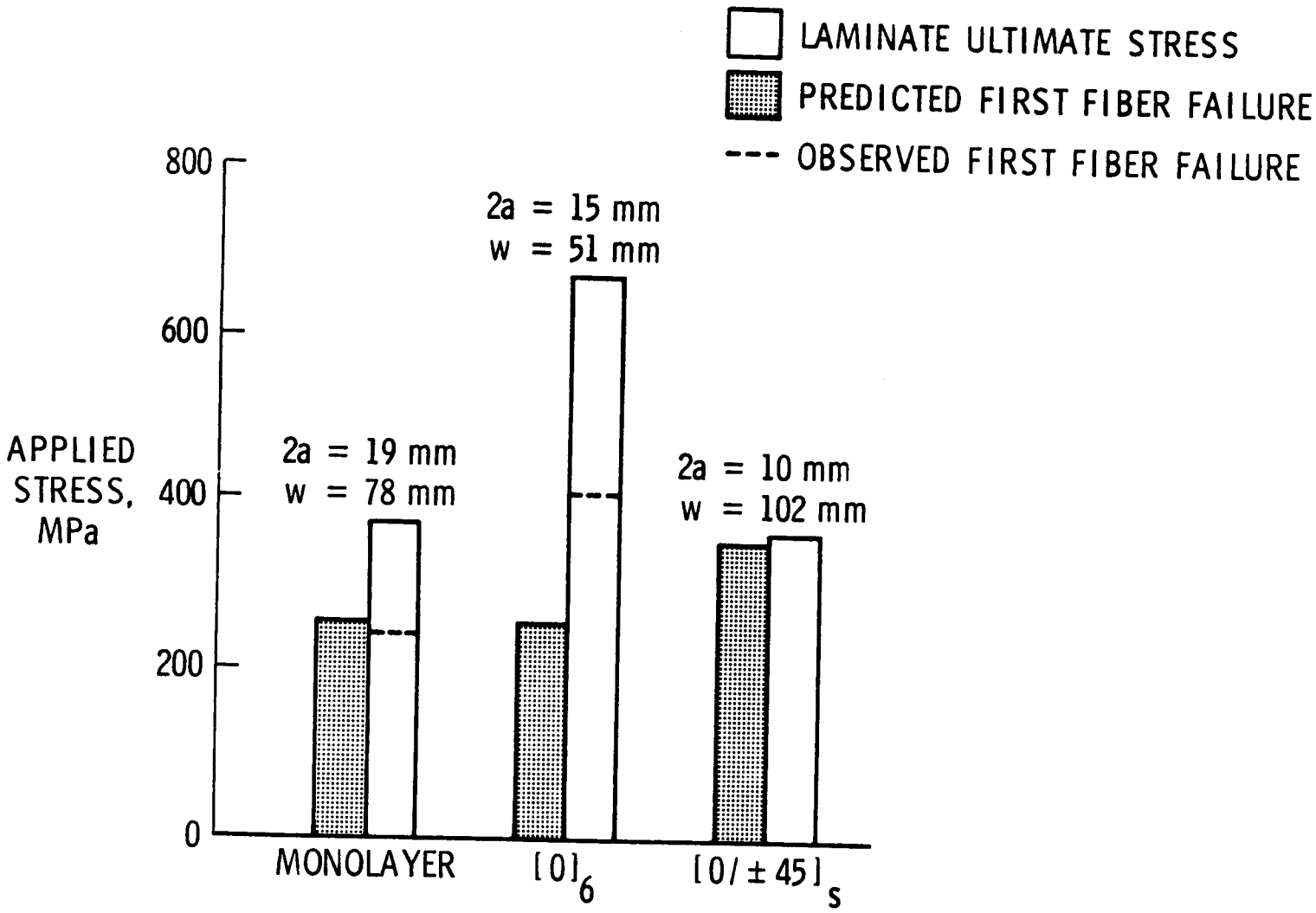

Figure 7. First fiber failure compared with laminate ultimate stress for specimens with crack-like slits.

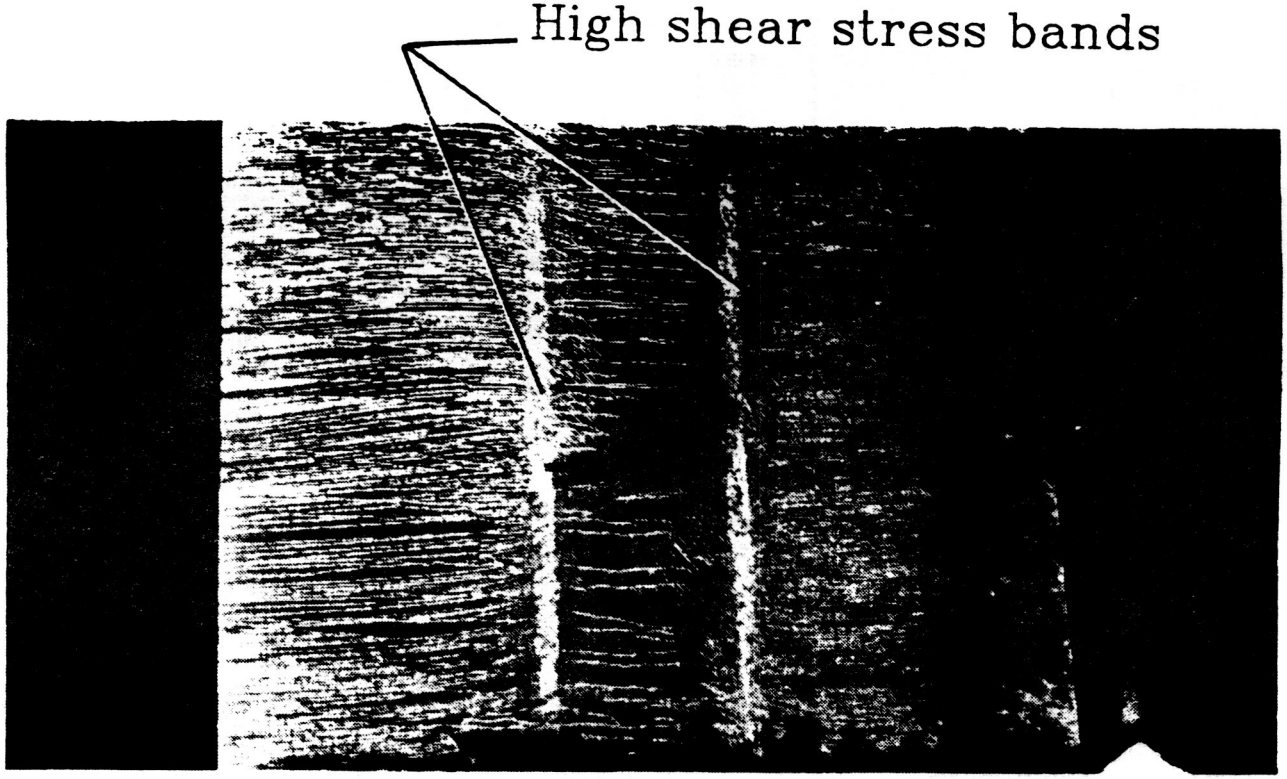

[Goree and Jones, Clemson Univ.]

Figure 8. Brittle lacquer crack pattern in boron/aluminum monolayer at 12,5000 N. Goree and Jones [7].

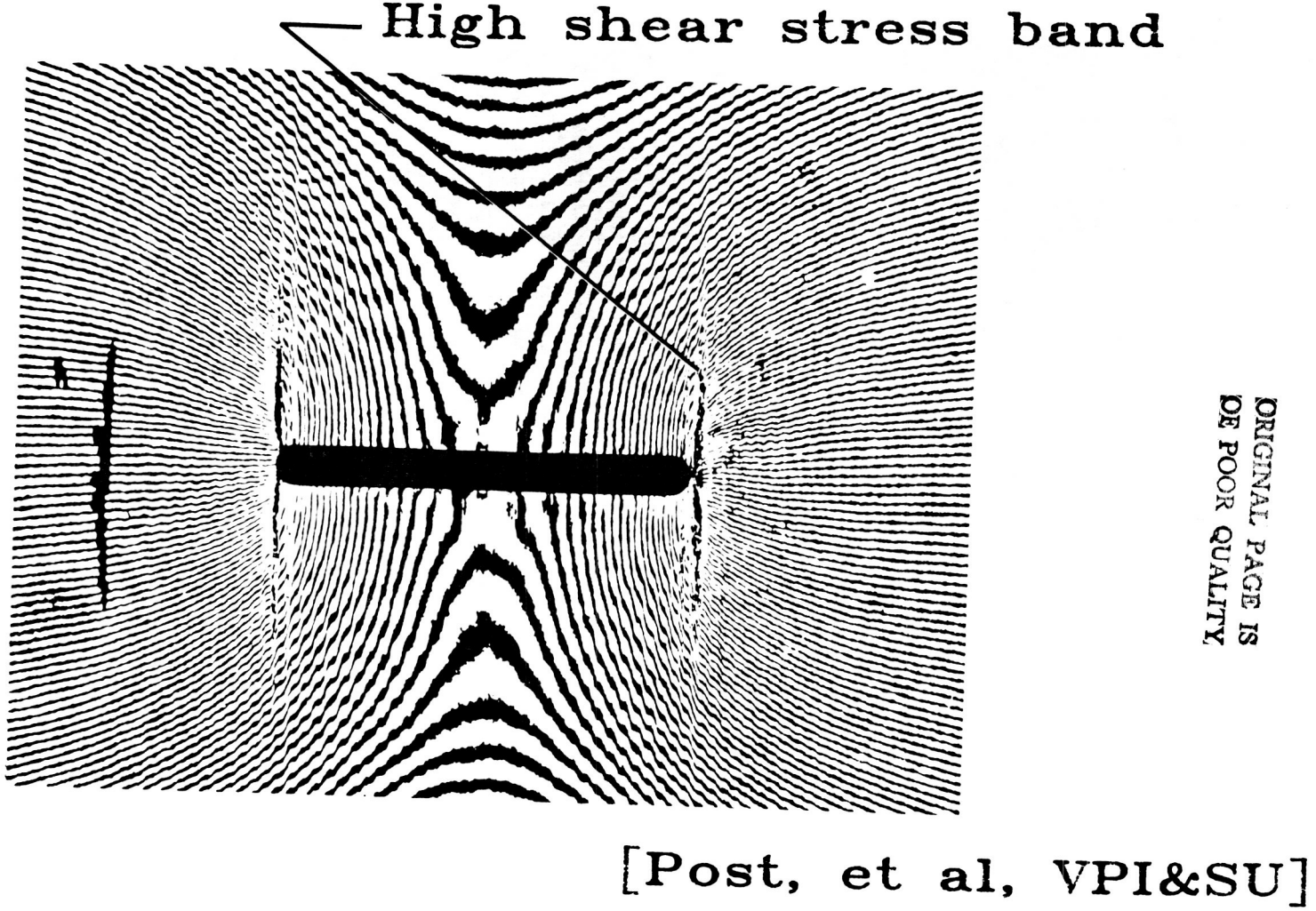

Figure 9. Moire fringes in a $[0/\pm45]_s$ boron/aluminum laminate. 2a = 5.5 mm, W = 14.7 mm. Post, et al. [8].

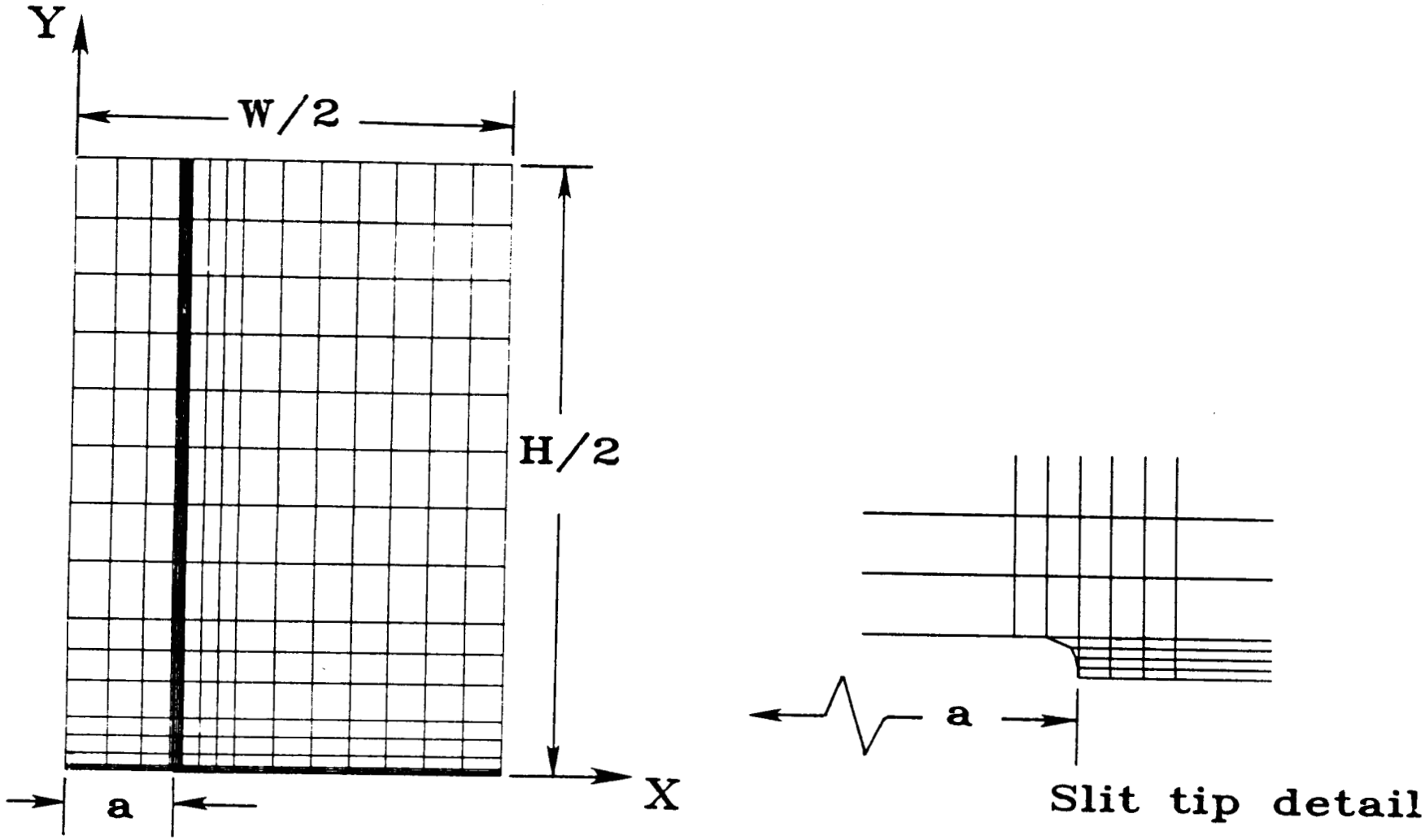

Figure 10. Rectangular mesh with curved slit tip. 2a = 19 mm, W = 78 mm, and H = 101 mm.

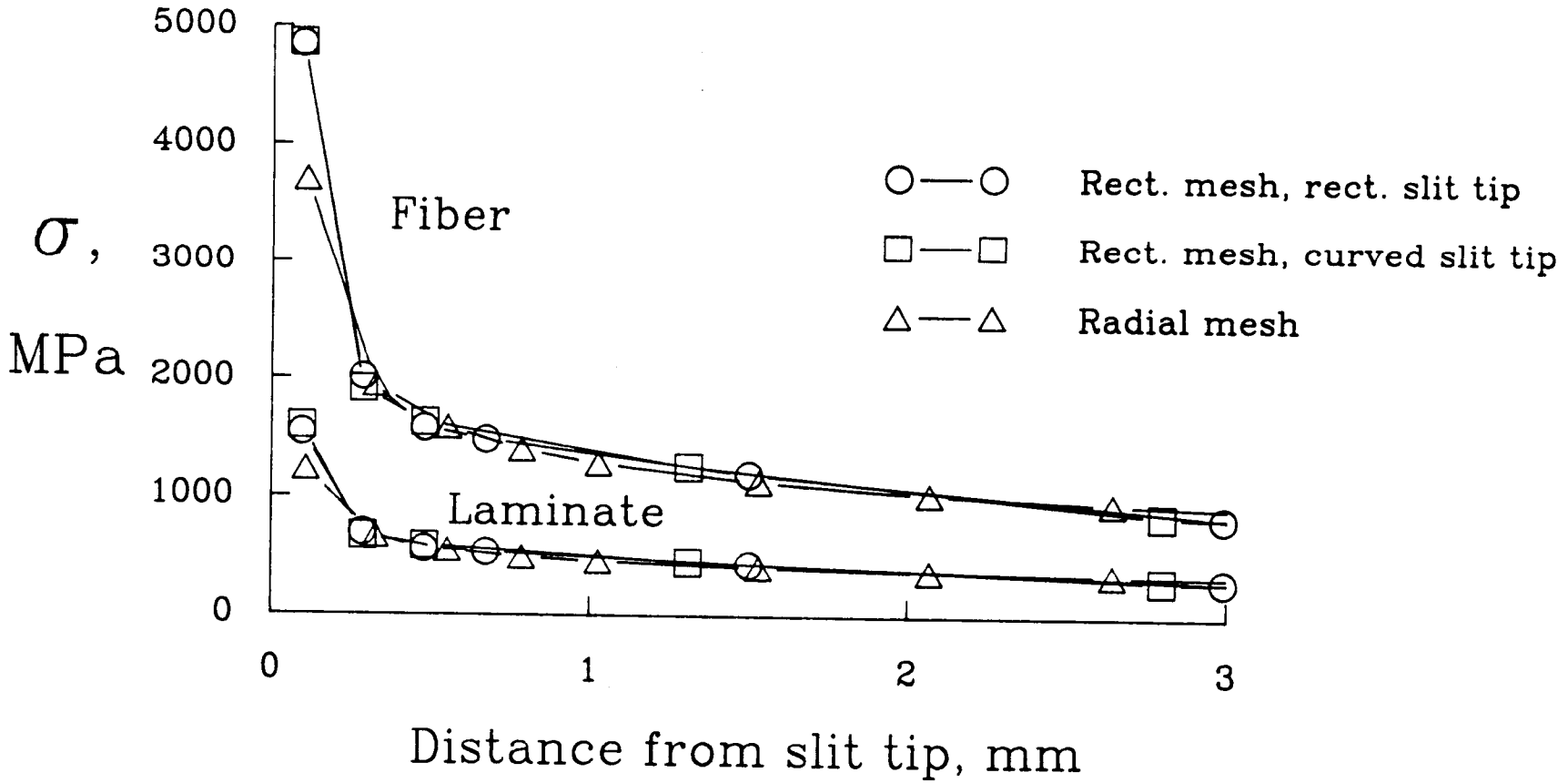

Figure 11. Fiber and laminate stress distributions ahead of slit tip for different meshes.

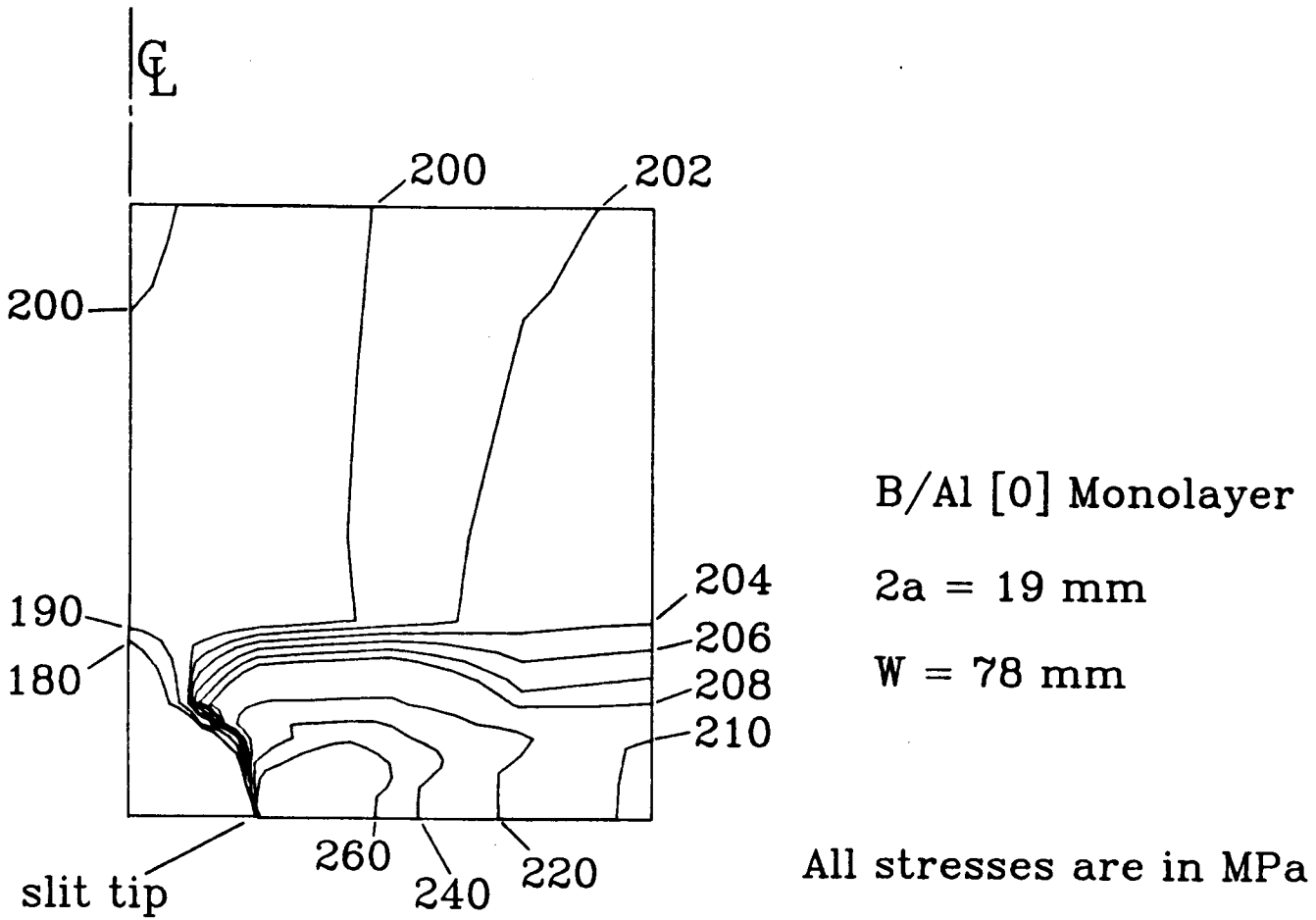

Figure 12. σ_y stress contours for boron/aluminum monolayer using radial mesh.

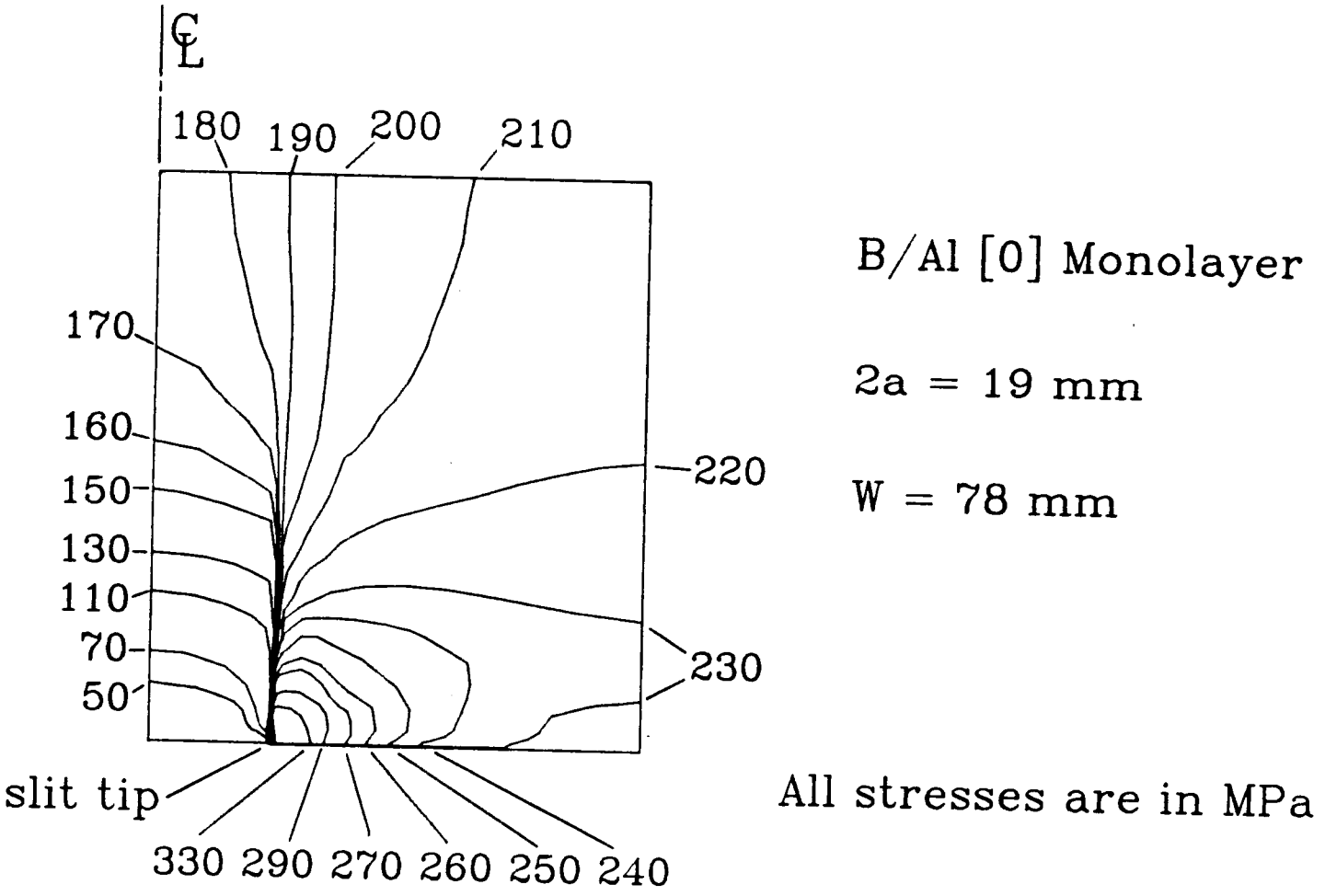

Figure 13. σ_y stress contours for boron/aluminum monolayer using rectangular mesh.

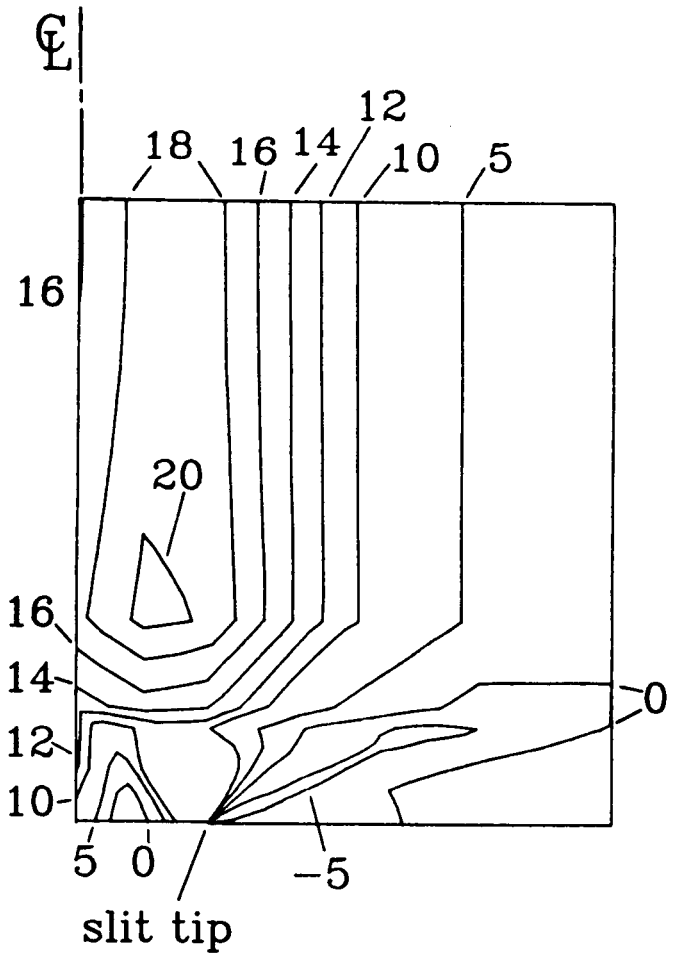

B/Al [0] Monolayer

2a = 19 mm

W = 78 mm

All stresses are in MPa

Figure 14. τ_{xy} stress contours for boron/aluminum monolayer using radial mesh.

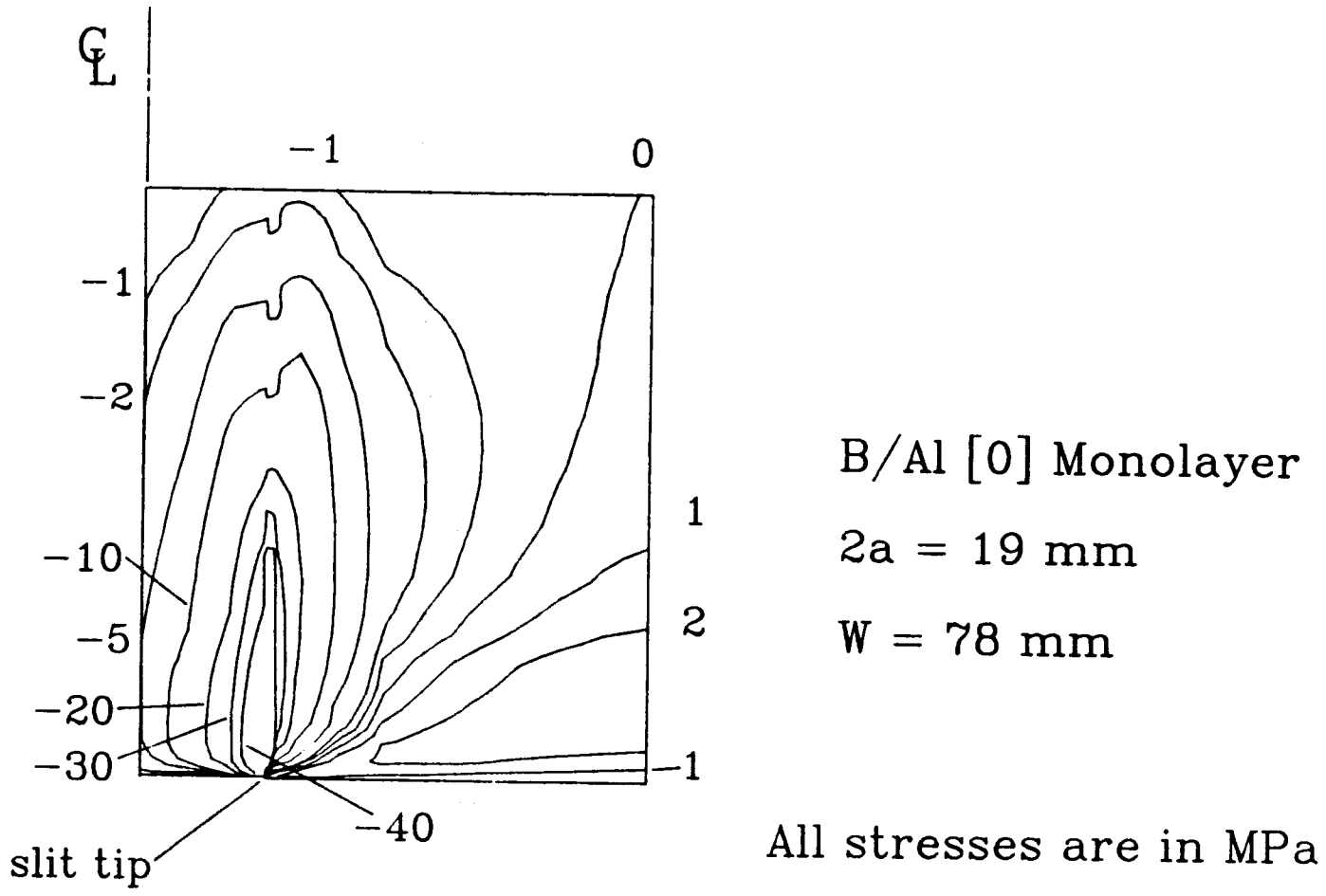

Figure 15. τ_{xy} stress contours for boron/aluminum monolayer using rectangular mesh.

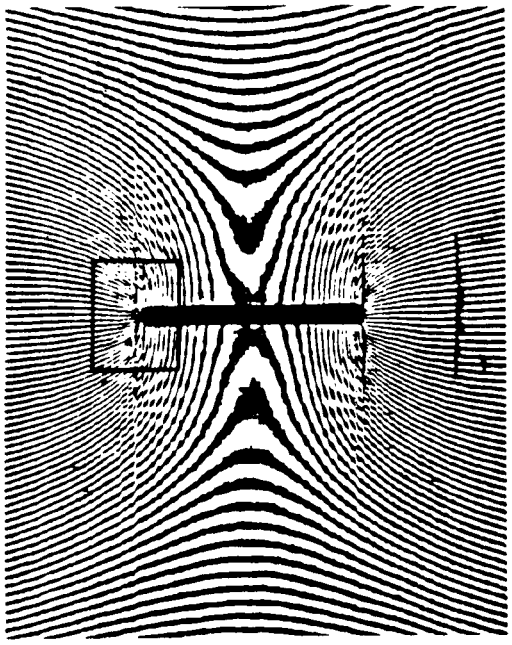

(a) Global pattern, $[0/\pm45]_s$.

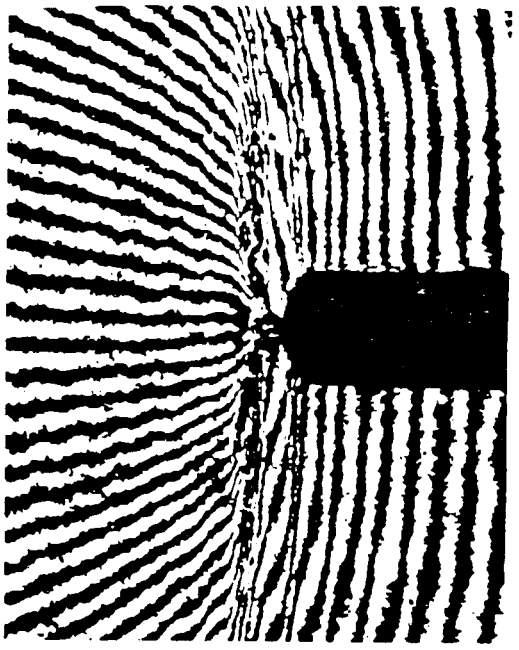

(b) Local pattern at slit tip, $[0/\pm45]_s$.

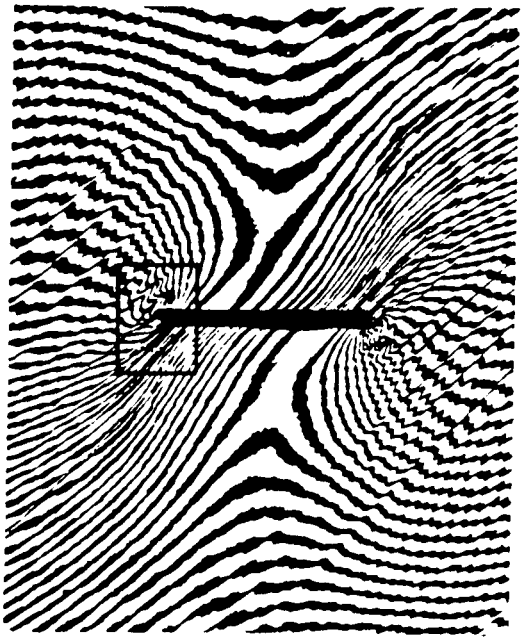

(c) Global pattern, $[\pm45/0_2]_s$.

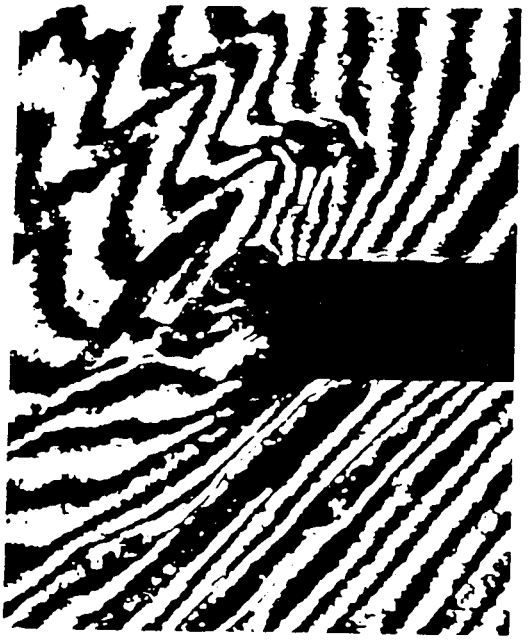

(d) Local pattern at slit tip, $[\pm45/0_2]_s$.

Figure 16. Moire fringe patterns for a $[0/\pm45]_s$ and a $[\pm45/0_2]_s$ boron/aluminum tensile specimen with a center slit. 2a = 5.5 mm, W = 14.7 mm. Guo, Post, and Czarnek [11].

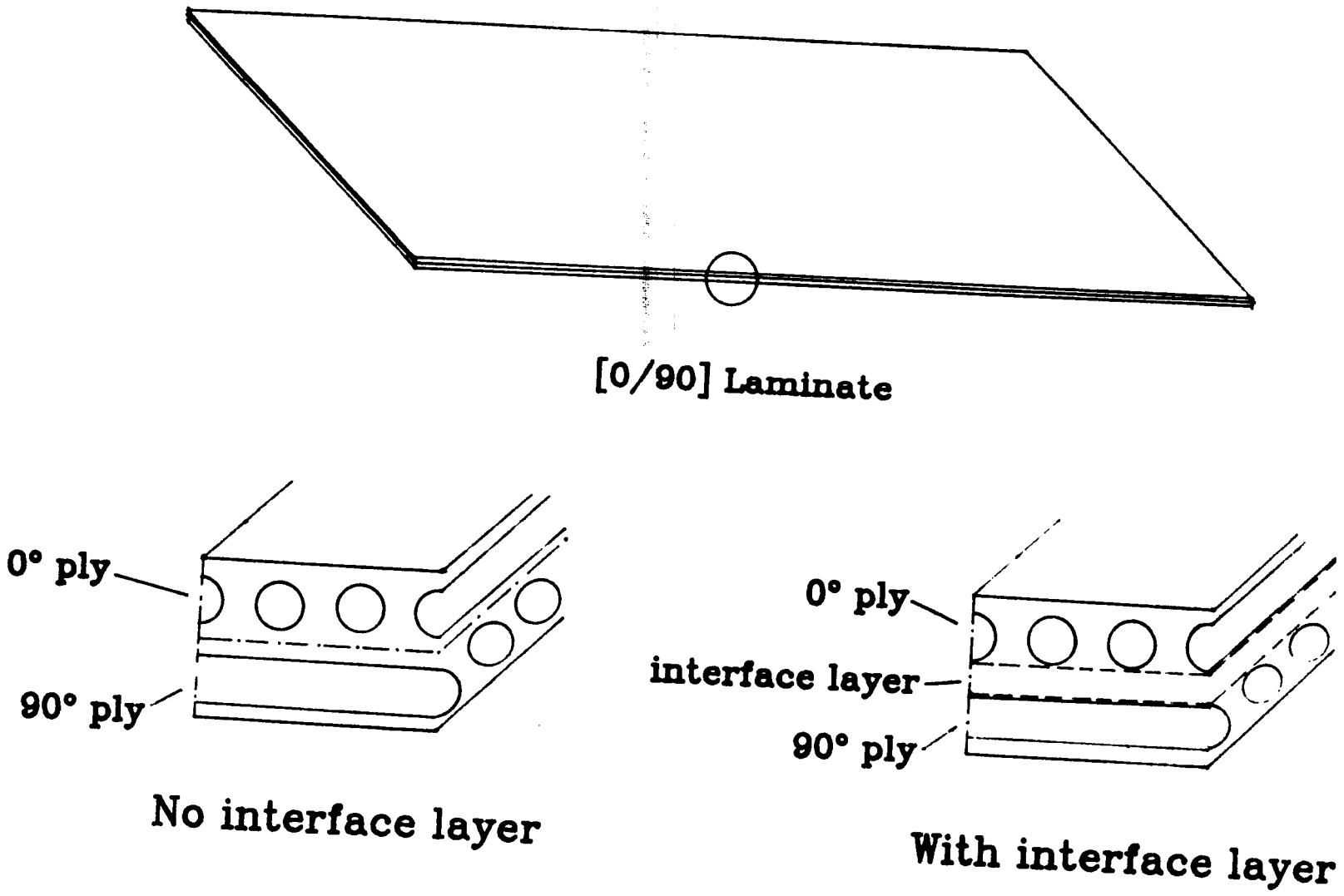

Figure 17. Interface modeling.

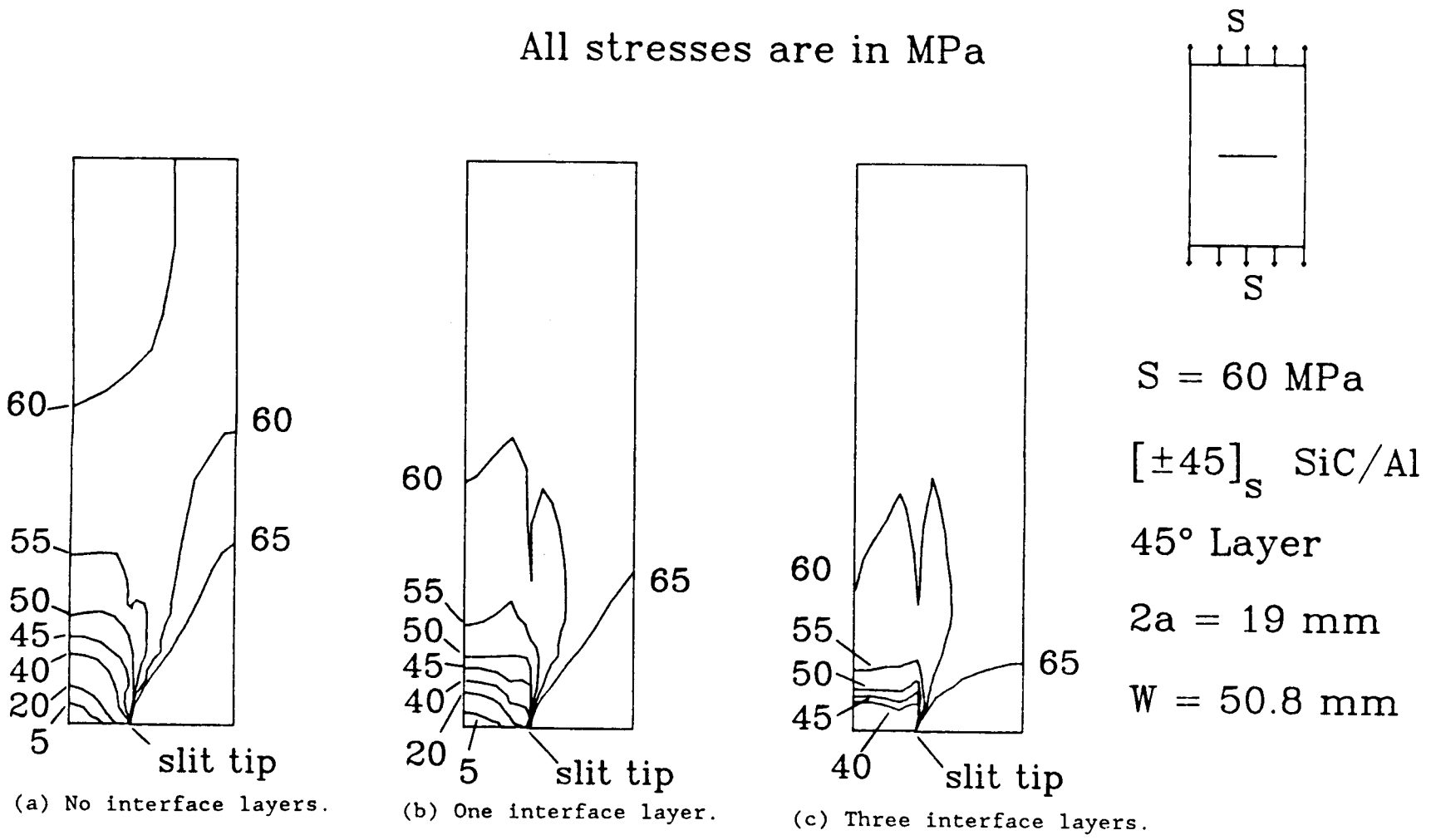

Figure 18. σ_y stress contours for 45° layer in $[\pm 45]_s$ laminate at applied stress of 60 MPa.

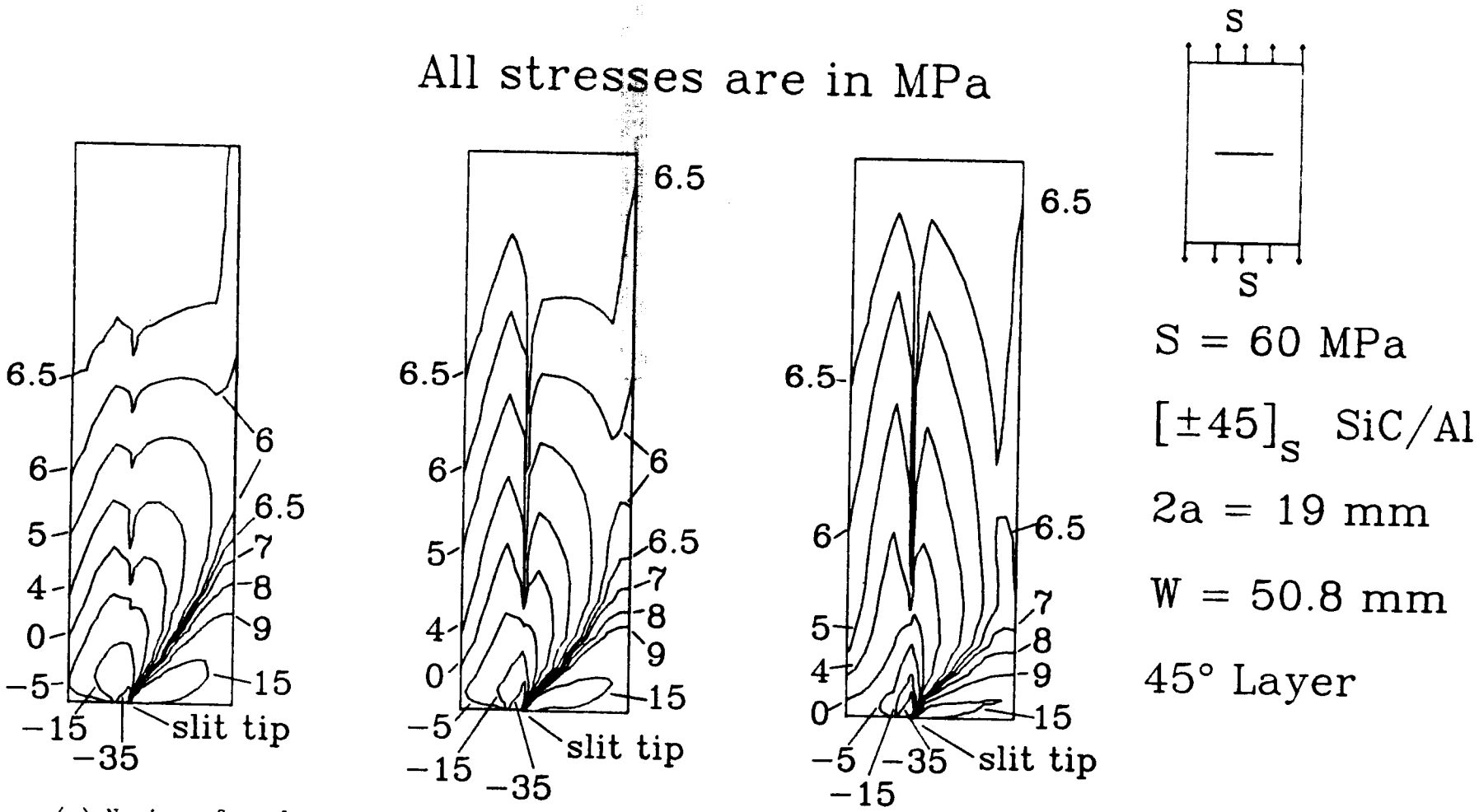

(a) No interface layers. (b) One interface layer. (c) Three interface layers.

Figure 19. τ_{xy} stress contours for 45° layer in $[\pm 45]_s$ laminate at applied stress of 60 MPa.

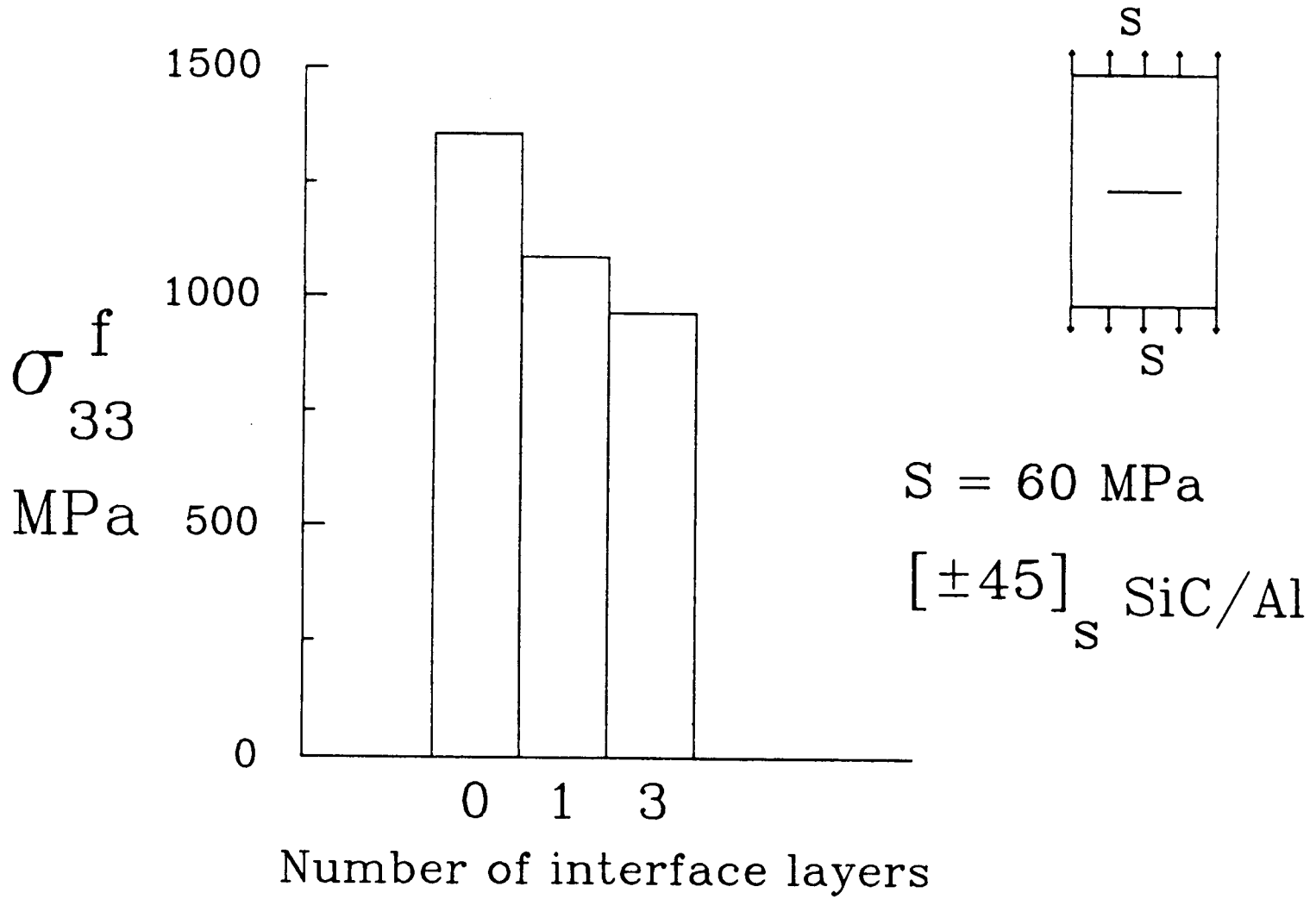

Figure 20. Fiber axial stresses at slit tip for $[\pm 45]_s$ laminate with interface layers at an applied stress of 60 MPa.

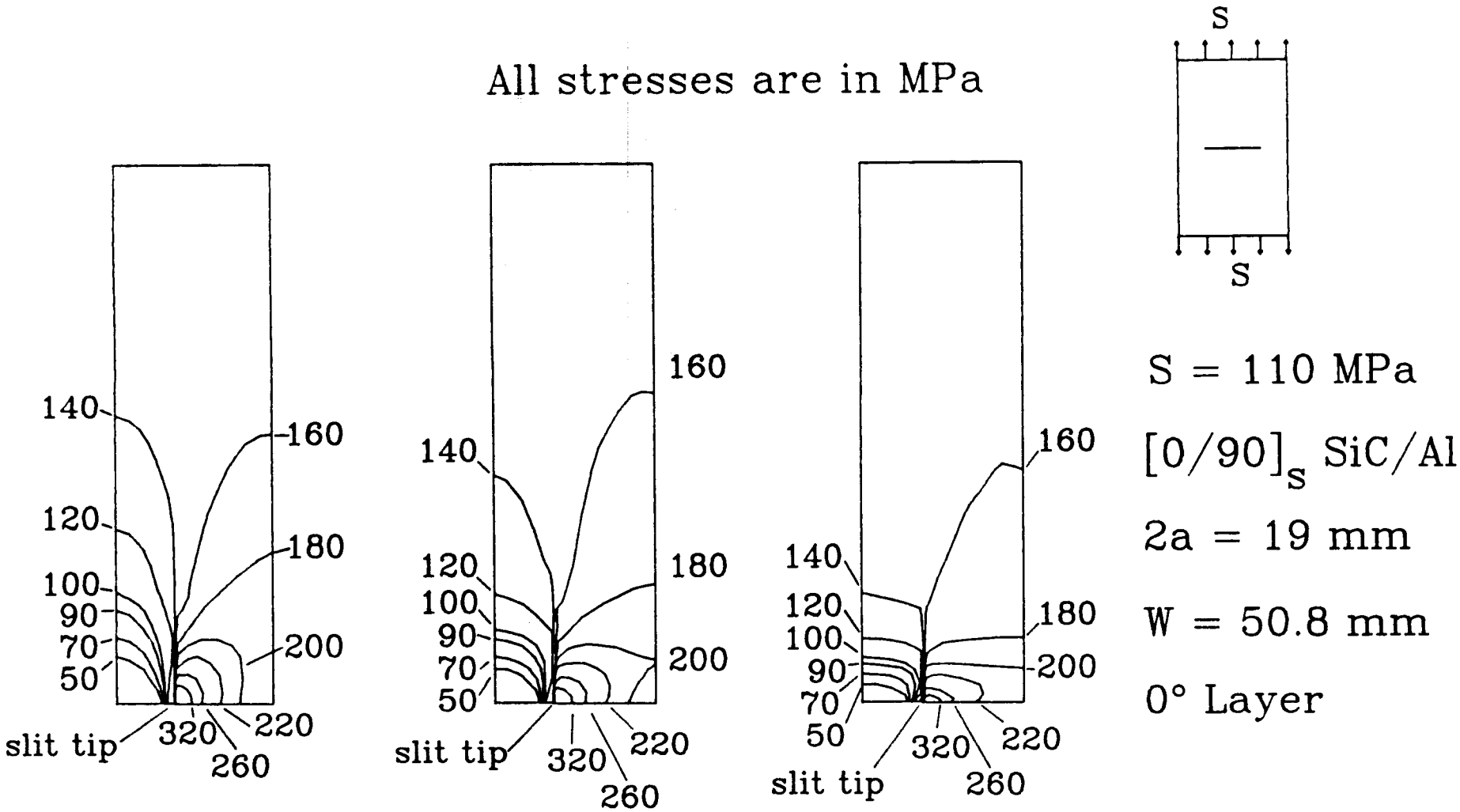

(a) No interface layers. (b) One interface layer. (c) Three interface layers.

Figure 21. σ_y stress contours for 0° layer in $[0/90]_s$ laminate at applied stress of 110 MPa.

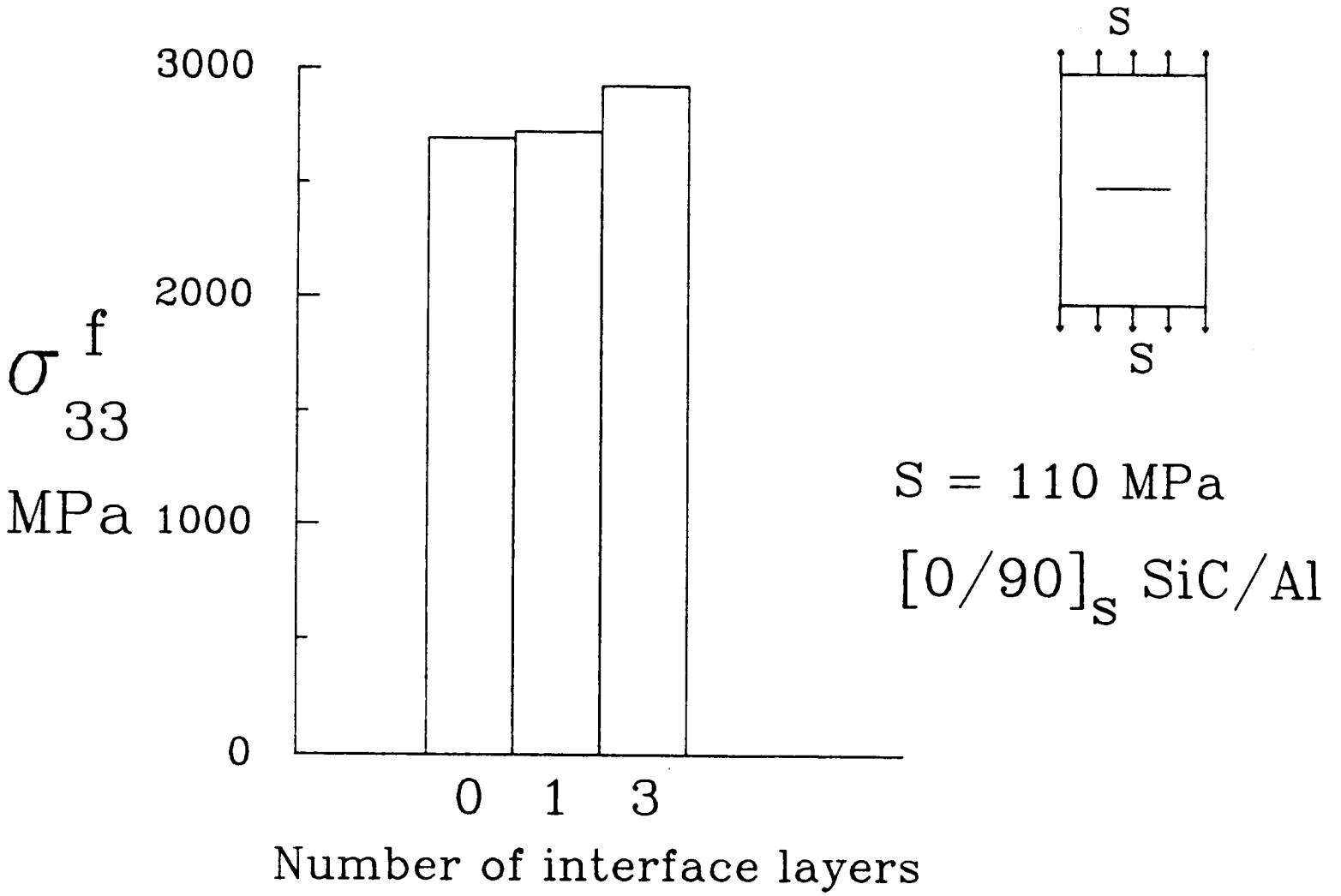

Figure 22. Fiber axial stresses at slit tip stress concentrations for $[0/90]_s$ laminate with interface layers at an applied stress of 110 MPa.

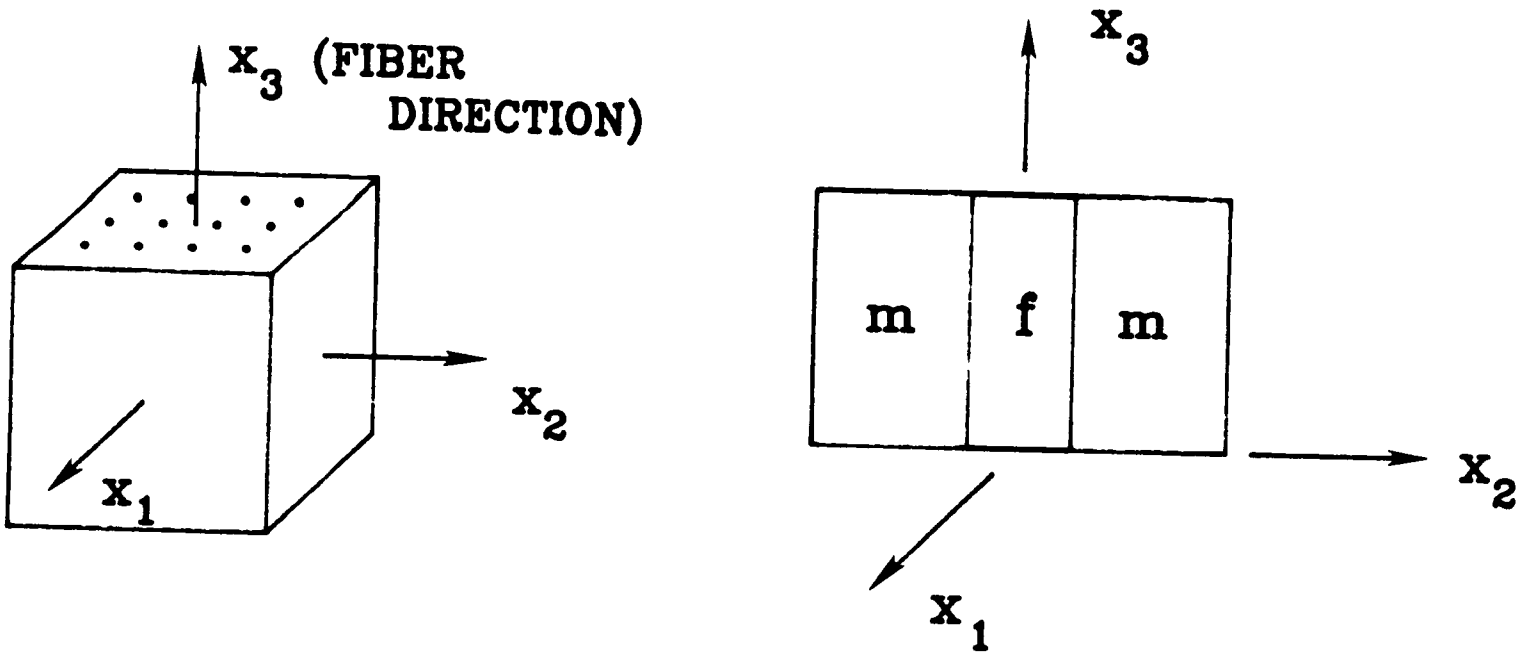

Figure 23. Element material model.

Report Documentation Page

1. Report No.	2. Government Accession No.	3. Recipient's Catalog No.
NASA TM-100629		

4. Title and Subtitle
Analysis of Notched Metal Matrix Composites Under Tension Loading

5. Report Date
June 1988

6. Performing Organization Code

7. Author(s)
C. A. Bigelow

8. Performing Organization Report No.

10. Work Unit No.
505-63-01-05

9. Performing Organization Name and Address
National Aeronautics and Space Administration
Langley Research Center
Hampton, Virginia 23665-5225

11. Contract or Grant No.

13. Type of Report and Period Covered
Technical Memorandum

12. Sponsoring Agency Name and Address
National Aeronautics and Space Administration
Washington, DC 20546

14. Sponsoring Agency Code

15. Supplementary Notes
This paper will also be published in an ASTM STP entitled "Metal Matrix Composites: Tesing, Analysis, and Failure Modes,"ASTM 1032, W. S. Johnson, Editor, 1989.

16. Abstract

This paper presents techniques based on a three-dimensional finite-element analysis for the analysis of continuous fiber reinforced metal matrix composites. Examples are shown for specific metal matrix composites such as boron/aluminum and silicon-carbide/aluminum.

Specimen stress-strain behavior and stress at first fiber failure were predicted for boron/aluminum laminates containing circular holes and crack-like slits. The predictions compared very well with test data for laminates containing 0° fibers and reasonably well for $[\pm 45]_{2S}$ laminates. Mesh configuration was shown to have an effect on the calculation of stresses local to the notch. The presence of thin interface layers of matrix material had a significant influence on the slit tip stress state, causing sharper stress gradients near the notch. Interface layers reduced the slit-tip fibers stresses in a $[\pm 45]_{S}$ silicon-carbide/aluminum laminate but increased them in a $[0/90]_{S}$ laminate.

17. Key Words (Suggested by Author(s))	18. Distribution Statement
Finite element analysis Three-dimensional elastic-plastic Fiber failure Stress contours	Unclassified - Unlimited Subject Category - 24

19. Security Classif. (of this report)	20. Security Classif. (of this page)	21. No. of pages	22. Price
Unclassified	Unclassified	42	A03